Seepage to Ditches and Topographic Depressions in Saturated and Unsaturated Soils

A. R. Kacimov[1], *Yu. V. Obnosov*[2], *and J. Šimůnek*[3]

[1]Department of Soils, Water and Agricultural Engineering, Sultan Qaboos University, Oman

ORCID ID: orcid.org/0000-0003-2543-3219

Emails: anvar@squ.edu.om, akacimov@gmail.com

[2]Institute of Mathematics and Mechanics, Kazan Federal University, Kazan, Russia,

ORCID ID: orcid.org/0000-0001-9220-7989

Email: yobnosov@kpfu.ru

[3]Department of Environmental Sciences, University of California Riverside, CA, USA

Email: jsimunek@ucr.edu

Abstract. An isobar generated by a line or point sink draining a confined semi-infinite aquifer is an analytic curve, to which a steady 2-D plane or axisymmetric Darcian flow converges. This sink may represent an excavation, ditch, or wadi on Earth, or a channel on Mars. The strength of the sink controls the form of the ditch depression: for 2-D flow, the shape of the isobar varies from a zero-depth channel to a semicircle; for axisymmetric flow, depressions as flat as a disk or as deep as a hemisphere are reconstructed. In the model of axisymmetric flow, a fictitious J.R. Philip's point sink is mirrored by an infinite array of sinks and sources placed along a vertical line perpendicular to a horizontal water table. A topographic depression is kept at constant capillary pressure (water content, Kirchhoff potential). None of these singularities belongs to the real flow domain, evaporating unsaturated Gardnerian soil. Saturated flow towards a triangular, empty or partially-filled ditch is tackled by conformal mappings and the solution of Riemann's problem in a reference plane. The obtained seepage flow rate is used as a right-hand side in an ODE of a Cauchy problem, the solution of which gives the draw-up curves, i.e., the rise of the water level in an initially empty

trench. HYDRUS-2D computations for flows in saturated and unsaturated soils match well the analytical solutions. The modeling results are applied to assessments of real hydrological fluxes on Earth and paleo-reconstructions of Martian hydrology-geomorphology.

Key Words:

Analytic and HYDRUS solutions for Darcian 2-D and axisymmetric flows in saturated and unsaturated soils towards drainage ditches and topographic depressions;

Evaporation and seepage exfiltration from shallow groundwater;

Complex potential and conformal mappings;

Method of images with sinks and sources for the Laplace equation and ADE;

Boundary value problems involving seepage faces on Earth and Mars;

Isobars, isotachs, constant piezometric head, and Kirchhoff potential lines.

"I had to live in the desert before I could understand the full value of grass in a green ditch."

Ella Maillart

1. Introduction

Analytical models of 2-D seepage towards drainage ditches and trenches, constructed by civil, geotechnical, and agricultural engineers, used the machinery of complex variables (Anderson, 2013, Aravin and Numerov, 1953, Bear, 1972, Kirkham and Powers, 1972, Polubarinova-Kochina, 1962,1977, hereafter abbreviated as PK-62,77, Skaggs et al., 1999, Strack, 1989, Vedernikov, 1939), in particular, by tackling free boundaries of Darcian flows, the so-called phreatic surfaces.

We recall (see, e.g., Radcliffe and Šimůnek, 2010) that transient, 3-D, saturated-unsaturated flows in porous media (when both water and soil are incompressible) obey the Richards equation:

$$\frac{\partial \theta}{\partial t} = \nabla\left(K(p)\nabla h\right) \tag{0}$$

where $\theta(t,x,y,Z)$ is the volumetric moisture content, ∇ is the nubla operator (in Cartesian or cylindrical coordinates), $K(p,x,y,Z)$ is the hydraulic conductivity function, $h(t,x,y,Z)=p+Z$ is the total head, p is the pressure head, Z is a vertical coordinate, and $p(\theta)$ is a capillary pressure (water retention) function, fixed for each soil. Eq. (0) involves the Darsy law $\vec{V}$=-$K(p)\nabla h$, where $\vec{V}$ is the Darcian flux vector, and the principal of mass conservation.

Boundary value problems (hereafter abbreviated as BVPs) are solved for eq. (0) by specifying initial conditions, e.g., $\theta(0,x,y,Z)$, as well as imposing physically meaningful boundary conditions (e.g., Dirichlet's, Neuman's). Only numerical codes like HYDRUS-3D (Šimůnek et al., 2016) tackle such problems for arbitrary 3D transient flows. Eq. (0) is a highly nonlinear parabolic PDE. For steady flows, its LHS vanishes, and the equation becomes elliptic. If the flow is purely saturated and the porous medium is homogeneous, then $K(p)=K_s$, where K_s is saturated hydraulic conductivity, and eq. (0) is reduced to a linear Laplace one. For a special class of soils with an exponential $K(p)$ function (Gardner, 1958), the Kirchhoff transform makes possible a linearization such that eq. (0) is reduced to a linear advective dispersion equation (ADE) with respect to a Kirchhoff potential. The ADE can be analytically solved for solitary or systematically placed singularities (Kacimov, 2007, Philip, 1968, 1971, Pullan, 1990, Raats, 1971, 1972). More details on BVPs for the Laplace equation and the ADE are given in Sections 2-5 of the MS.

The total head for saturated seepage in undeformable porous media obeys the Laplace equation and, therefore, the mathematical commonality between flows of ideal fluids (Zhukovskii, 1948) and pore water motion has been widely explored (PK-62,77, Strack,1989). The method of images and the theory of BVPs (Henrici, 1993) have been engaged. In this paper, we combine these traditional analytical and new numerical (HYDRUS-2D, Šimůnek et al., 2016) methods to problems of groundwater and soil water movement from shallow confined and unconfined aquifers

towards ditches and topographic depressions, common in desert landforms of arid-hyperarid climates of Oman and Mars.

A practical motivation of our work stems from a daunting problem of groundwater inundation caused by a rapid rise of the water table in perched unconfined and shallow confined aquifers, detected in many urban areas of the world (see, e.g., Attard et al., 2016, Barron et al., 2013, Chaudhary, 2012, Coda et al., 2019, Howard and Israfilov, 2012, Jha et al., 2012, Kazemi, 2011, Lerner, 2003, Lerner and Harris, 2008, Medovar et al., 2018, Naik et al., 2008, Porse et al., 2016, Preene and Fisher, 2015, Quan et al., 2010, Schirmer et al., 2013, Vázquez-Suñé et al., 2005, Vogwill, 2016). Surprisingly, the arid countries of Arabia – despite the hydrological mantra on water deficit and groundwater depletion – encounter the same problem of waterlogging of urban structures by shallow groundwater as the cities in humid zones (e.g., Abu-Rizaiza et al., 1989, Abu-Rizaiza, 2006, Al-Rawas and Qamaruddin, 1998, Al-Sefry and Şen, 2006, Al-Senafy, 2011, Al-Senafy et al., 2015, Bob et al., 2016, Kreibich and Thieken, 2008). It is noteworthy that urbanization in the Southwest of the USA caused similar negative hydrological impacts (amplification of flash flood intensities due to reduced evapotranspiration, see, e.g., Goudie, 2013).

In the metropolitan area of Muscat, at the campus of Sultan Qaboos University (SQU), the groundwater inundation has become evident even without any piezometry. In recent years, subsurface water seeped out in natural topographic depressions, man-made excavations, ditches, and drainage channels called wadis. Large wet spots or ponded areas at SQU are bio-marked by adjacent lush, wild vegetation. In the desert climate of Oman, this vegetation in some places pops up virtually as Maillart's "grass in green ditches" (see the epigraph). The studied SQU field is located in a hyperarid zone of the Batinah Coast, Oman, Arabia (e.g., Alsharhan et al., 2001). The investigated wadi section was about 1 km long, with several excavated pits-trenches and natural depressions. For instance, one of the excavations has the following coordinates: Northing: 619721, Easting: 2608729, 47.5 m above the level in the Sea of Oman. Urbanization of the field started in

the mid-1980s, before which the site was a desert with scattered shrubs and trees. Currently, a significant part of the campus area is paved, which reduced natural evapotranspiration. Waterlogging and associated lush vegetaiton is, geotechnically deleterious, putting footings of the SQU buildings, roads, subsurface cables, etc., in jeopardy, even when the salinity of the rising groundwater is small. Secondary salinization of the topsoil is also widespread in Oman when the draw-up of the water table is from an aquifer of poor groundwater quality. Fieldwork has been carried out in November-June 2020 at the SQU campus: auger holes, ditches, and excavations have been constructed, and groundwater monitored, to assess soil moisture oozing fluxes above shallow perched and confined aquifers detected in the study area.

The motivation of this work also stems from our intention to attract the attention of Planet Mars hydrologists, who model seepage of Martian groundwater into remotely scanned relief features of the Red Planet, to the legacy of experts in irrigation and drainage engineering, who – during the 20th century - assembled a good arsenal of analytical and numerical methods for investigations of the motion of pore water towards drains (Bear, 1972, Kirkham and Powers, 1972, Skaggs et al., 1999, 2012, Strack, 1989, Vedernikov, 1939, Zhukovskii, 1948).

Mars is a hyperarid planet where the remotely analyzed landforms (craters, dunes, endorheic lakes and playas, pits, alcoves, gullies, recurring slope lineae, fluvio-lacustrine basins, fans, shallow dust horizons, streaks, amphitheater-headed valleys, sapping valleys, etc.) and hydrological elements (springs, outseeps, deep fracture conduits, seepage spots), which convey liquid water, brine, and Martian gases are studied. The alleged paleo and current dynamics of Martian pore fluids are elaborated, for example, in Abotalib and Heggy (2019), Bhardwaj et al. (2019), Boatwright and Head (2019), Edwards and Piqueux (2016), Goldspiel and Squyres (2011), Grimm et al. (2014), Hobbs et al. (2014), Kereszturi et al. (2011), Kochel and Piper (1986), Luo et al. (2011), Malin and Carr (1999) Malin and Edgett (2000), Marra et al. (2014, 2015), Michalski et al. (2013), Mukherjee et al. (2020), and Salese et al. (2019).

For hypothetical Martian aquifers (both unconfined and artesian), K_s is assessed from proxy data (see, e.g., the posited "nominal" value in Goldspiel and Squyres (2011); Luo et al. (2011) evaluated the hydraulic conductivity from the solution of inverse problems of the hydrological cycle on Mars; Boatwright and Head (2019) assumed that the conductivity exponentially decreases with the Martian depth). We note that even the Darcy law is sometimes not correctly formulated by Martian hydrologists (see, e.g., an erroneous eq. (1) in Abotalib and Heggy, 2019). On Mars, purely unsaturated flows are also hypothesized (Edwards and Piqueux, 2016, Grimm et al., 2014), but – to the best of our knowledge - Martian hydrologists (e.g., Luo et al., 2011) so far have used only flow models for saturated soils.

Models of Darcian flows towards drainage ditches commonly conceptualize the ditches as rectangles in vertical cross-sections having vertical slopes (Afruzi et al., 2014, Barua and Alam, 2013, Chahar and Vadodaria, 2008, Gureghian and Youngs, 1975, Sarmah and Tiwari, 2018, Youngs, 1975, 1990, 1994). However, natural ephemeral river channels, both on Earth and Mars, as well as constructed drainage ditches and trenches often have non-rectangular shapes (Grotzinger et al., 2014, Kocurek et al., 2020). Excavations (pits) and natural depressionsare often axisymmetric and mild-sloped (see, e.g., Goldspiel and Squyres, 2011). Only in few studies have phreatic seepage and flows in the unsaturated zone to non-rectangular (trapezoidal and curvilinear) draining entities been analytically examined (PK-77 reported solutions by Bazanov, p. 150 of her book, and Vedernikov, pp.181-182, see also Ilyinsky and Kacimov, 1992a, Kacimov, 2005, 2006a, Kacimov and Obnosov, 2002). We note that although Luo et al. (2011) sketched trapezoidal draining channels in their models of groundwater discharge into these channels, they posited the Dupuit-Forchheimer (hereafter abbreviated as DF) model, which actually ignores the shape of channels. Marra et al. (2014, 2015) conceptualized, and studied experimentally in sand boxes, seepage into real trapezoidal channels, allegedly occurring on Mars, but unfortunately did not refer to a plethora

of theoretical studies of this type of seepage to draining channels on our own planet (see, e.g., Aravin and Numerov, 1953, PK-62,77, Vedernikov, 1939).

This work is organized as follows. In Section 2, we develop a simple analytical solution for a 2-D (not DF!) confined flow to a curvilinear ditch draining a saturated, confined aquifer. Some natural wadi channels in our study area are arcuate, like ones on Mars (Malin and Carr, 1999), but as the first approximation, we ignore the 3-D effect. Our isobaric ditch contour is an isobar generated by a line sink. In Section 3, we obtain a similar solution for a point sink in an axisymmetric flow towards a crater-shaped isobar, the piezometric head being still a harmonic function. In Section 4, we assemble an infinite array of J.R. Philip's sinks-sources of the advective dispersion equation (ADE) for the Kirchhoff potential, which models an axisymmetric, steady water movement from a horizontal water table towards a topographic depression in a partially saturated so-called Gardner soil. In Section 5 and Appendix I, 2-D seepage towards a triangular empty or partially-filled ditch is studied by the machinery of holomorphic functions. All analytical solutions of Sections 2-5 are tested against HYDRUS-2D numerical simulations. In Section 6, we outline applications to arid zone hydrology, and in particular, to Martian hydrology.

2. A Line-Sink-Generated Seepage Face Ditch Draining a Confined Aquifer

Unlike Hobbs et al. (2014) who could not identify confining layers, in the form of bedrocks and caprocks, of hydrostratigraphic units in the Martian regolith massif, we - when making excavations on our SQU site - indeed crashed a low-permeable caliche layer at a depth of 1.5-2 m. Typical values of K_s for low-permeable (cemented) layers (also called calcrete, petrocalcic horizons, see, e.g., Duniway et al., 2010), formed by the precipitation of carbonates or gypsum due to intensive evaporation in semi-arid, arid and hyper-arid regions, are given in the literature: 10^{-4} to 10^{-6} cm/s (Al-Yaqout and Townsend, 2004), 0.0002 to 0.008 m/day (Heilweil and Watt, 2011),

170 $2.8*10^{-7}$ m/s (Mujica and Bea, 2020), among others. In most reported cases, these strata
171 hydrologically cap the vadose zone rather than a perched or confined aquifer in our situation.

172 We could not excavate deeper to the next low-permeable horizon, and therefore, in Fig. 1a,
173 the aquifer is not confined from below. We note that genesis of the caliche in the SQU soil profile is
174 similar to what Michalski et al. (2013) argued about the impact of the upwelling Martian
175 groundwater on the sequence of cemented sediments of the Red Planet. Specifically, a periodic
176 "upwelling" (rise) of groundwater in SQU shallow perched unconfined aquifers, and intensive
177 evaporation from the water table has – allegedly – formed the caliche and "self-confined" this
178 aquifer by a caprock (Fig. 1a). When we "punctured" the caliche by the JCB scoop, groundwater
179 gushed into the excavation and filled it to the level of h_A^* (Fig. 1a) within 2 hours.

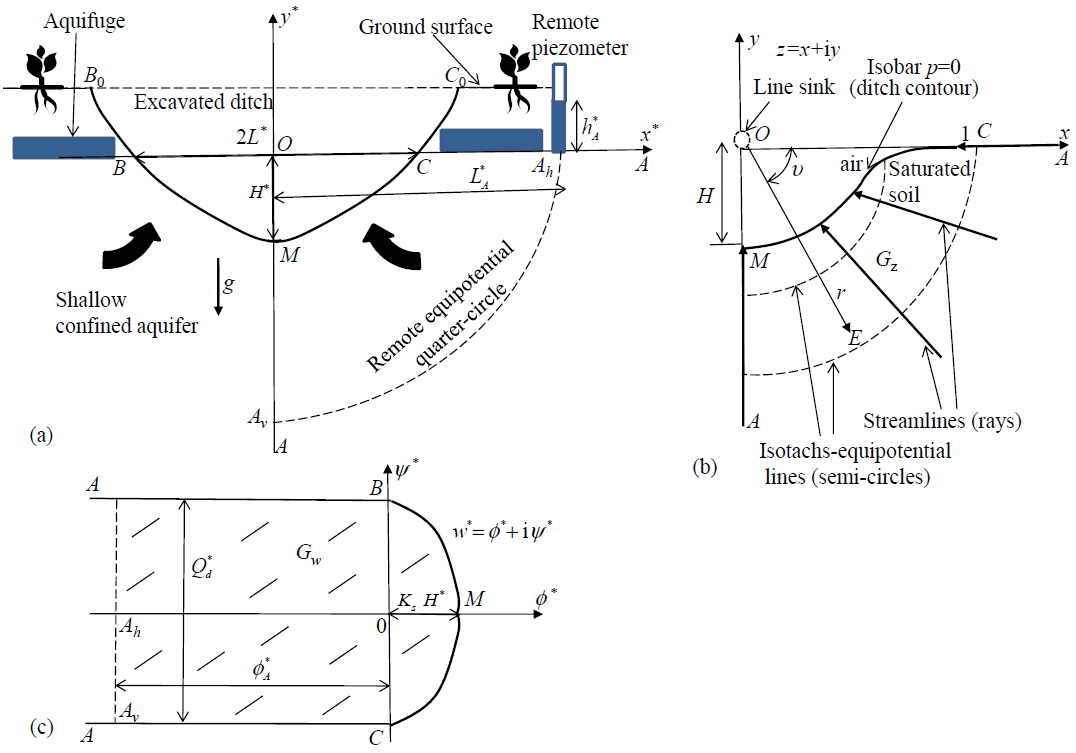

180

181 Fig. 1. A vertical cross-section of an empty ditch B_0MC_0 a); the right half of the empty ditch
182 constructed such that the bottom of the ditch, *BMC*, is a seepage face of the flow in the domain G_z,
183 generated by a fictive line sink at the origin O(*x*,*y*) b); the complex potential domain G_w for the
184 whole ditch c).

185

186 Fig. 1a shows a vertical cross-section of an empty ditch B_0MC_0, which drains a dry soil layer
187 above a horizontal aquifuge and a confined, homogeneous and isotropic aquifer (having at
188 saturation a hydraulic conductivity K_s) beneath an originally impermeable layer (caprock) *ABCA*.
189 Point *A* in Fig. 1a is at infinity on the Riemann sphere. If the excavation depth H^*, counted
190 from *ABCA* (point *M* is the deepest point of the ditch), is below the aquifuge, groundwater
191 discharges into the ditch *BMC* (symmetric and having the width 2 *L*) with the total flow rate Q_d^*
192 (m^2/s).
193 We assume that flow takes place only below the aquifuge. Goldspiel and Squyres (2011)
194 call this layer "aquiclude", that is – in the vernacular of groundwater hydrology (Strack, 1989) – a
195 "Martian misnomer," because Goldspiel and Squyres (2011) model impermeable rather than leaky
196 confining layers. At a point A_h (Fig. 1a), located a certain distance L_A^* ($L_A^* >> L$) from O, a remote
197 piezometer shows an elevation h_A^*. For simplicity, we ignore groundwater exfiltration upward
198 through the caliche in Fig. 1a, i.e., leaky layer (aquitard) flow scenarios, as considered by Kacimov
199 and Obnosov (2008, 2019).
200 We introduce Cartesian coordinates Ox^*y^* and the complex physical coordinate $z^* = x^* + \mathrm{i}\, y^*$
201 (Fig. 1b). In this section, we study the case of an empty ditch, i.e., the pressure head, p^*, along
202 *BMC* is zero. The emptiness of the ditch can be ensured by either a high Manning slope in the
203 direction perpendicular to the plane of Fig. 1a, so that all seeped water rapidly flows away as
204 surface water (see, e.g., Al-Shukaili et al., 2020a), or due to intensive evaporation, provided H^* is
205 relatively small and climate is arid enough. We note that surface water flow perpendicular to the
206 plane of Fig. 1, i.e., along the ditch, can be easily tracked on Earth. In our fieldwork, we detected
207 what Malin and Edgett (2000) called a Martian "seepage-fed surface runoff," slow Hortonian
208 motion downslope a ditch, with velocities of few mm/s. On Mars, the juxtaposition of groundwater

and surface water flows, reconstructed from the contemporary Martian landforms, is purely hypothetical (Malin and Carr, 1999).

As we have already pointed out in Section 1, a saturated 2-D flow from a homogeneous aquifer into a ditch (Fig. 1a) obeys Laplace':

$$\Delta h^*(x^*, y^*) = 0, \tag{1}$$

where $\vec{V}^*(u^*, v^*) = -K_s \nabla h^*$ is the Darcian velocity vector, u^* and v^* are its horizontal and vertical components, h^* is the total piezometric head, $h^* = p^* - y^*$, where the pore water pressure is $P^* = \rho_d g\, p^*$, g is gravity acceleration (9.8 m/s^2 on Earth and 3.7 m/s^2 on Mars), and ρ_d is pore fluid's (groundwater, brine, soil moisture) density. We emphasize that eq. (1) and all the results below do not assume a quasi-horizontal pore water motion, as it is postulated, for instance, in the DF model of Boatwright and Head (2019), and Luo et al. (2011).

We collected soil-sediment samples, measured K_s using standard techniques (see, e.g., Al-Shukaily et al., 2020b), and ascribed the obtained value to the textural class of HYDRUS-2D sands.

We introduce the complex potential $w^* = \phi^* + \mathrm{i}\psi^*$, $\phi^* = -K_s h^*$. The stream function ψ^* and a velocity potential ϕ^* are conjugate harmonic functions. Due to symmetry, we consider only the right half of the physical domain G_z (Fig. 1b). The following dimensionless quantities are introduced:

$$(H, L_A, x, y, z, r, h, h_A, p) = (H^*, L_A^*, x^*, y^*, z^*, r^*, h^*, h_A^*, p^*)/L, \quad (w, Q_d) = (w^*, Q_d^*)/(K_s L),$$

$$(V, u, v) = (V^*, u^*, v^*)/K_s$$

where r $(0 \le r < \infty)$ is the modulus of point $z = x + \mathrm{i}\, y$ in the aquifer (Fig. 1a)

The complex potential domain G_w is depicted in Fig. 1c. The piezometric head is assumed to be zero at points *B* and *C*. The image of the *BMC* isobar in *G* is a specific curve whose shape is

231 unknown. Far away from the ditch, the piezometric head is constant (h_A) along a circle of a radius
232 L_A in G_z (Fig.1a). The image of this circle is a segment A_hA_v in G_w (Fig. 1c).

233 Now we use the trick implemented by Zhukovskii (1948) in fluid mechanics of ideal fluids
234 (see recent applications in Belotserkovsky and Lifanov, 1992), also employed in problems of
235 subsurface mechanics of steady and transient Darcian flows (Fujii and Kacimov, 1998, Kacimov,
236 1992, 2000a, 2007, 2009, Kacimov et al., 2009, Kacimov and Obnosov, 2002, PK-62,77, Strack,
237 1989, 2020, Vedernikov, 1939). We place a line sink of intensity $Q=2Q_d$ at the origin of
238 coordinates. The complex potential of this sink is:

239
$$w = -\mathrm{i}\frac{Q_d}{2} - \frac{Q_d}{\pi}\mathrm{Ln}\, z, \quad z = r\exp[\mathrm{i}\,\nu], \quad r = \sqrt{x^2 + y^2},$$
$$h = \frac{Q_d}{\pi}\mathrm{Ln}\, z, \quad \psi = -\frac{Q_d}{2} - \frac{Q_d}{\pi}\theta, \quad |\mathrm{V}| = \frac{Q_d}{\pi r}, \tag{2}$$

240 where ν is the argument of z. It is evident from eq. (2) that the streamlines of this flow are rays
241 converging to point O in Fig. 1b. The isotachs and equipotential lines are semicircles centered at the
242 same point.

243 Now we restrict r in eq. (2) to only a positive-pressure part of the half-plane in Fig.1a, i.e.,
244 we use eq. (2) for the reconstruction of *BMC* by plotting the curve, which is determined by the
245 following explicit formula:

246
$$Q_d \mathrm{Ln}\sqrt{x^2 + y^2} = \pi y, \quad 0 \le x \le 1, \quad -H \le y \le 0. \tag{3}$$

247 The depth H of the ditch, found from the solution of the equation

248
$$Q_d\,\mathrm{Log}\,|y| = \pi y, \tag{4}$$

249 is equal to

250
$$H = -Q_d W(-\pi / Q_d)/\pi, \tag{5}$$

251 where W stands for the Lambert W-function (implemented as **ProductLog** in Wolfram's (1991)
252 *Mathematica*).

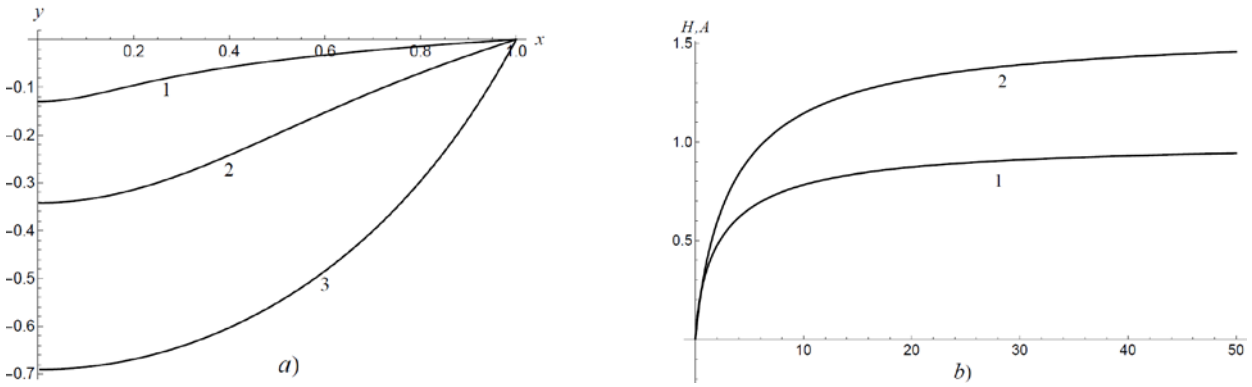

Fig. 2. a) Half-contours of sink-generated ditches for Q_d = 0.2, 1, and 5.86 (curves 1, 2, and 3, respectively). b) The depth H of a sink-generated ditch and its area A (curves 1 and 2, respectively) as functions of the seepage flow rate Q_d.

Fig. 2a shows the *MC* contours for sink-generated ditches (Fig. 1b) plotted for Q_d = 0.2, 1, and 5.86 (curves 1, 2, and 3, respectively). Curve 1 in Fig. 2b shows $H(Q_d)$. From eq. (3) it is obvious that for small Q_d, the ditch degenerates into a horizontal segment, while in another limit, $\lim_{Q_d \to \infty} H = 1$, *BMC* becomes a semicircle. The analytical solution (2)-(5) is similar to those obtained by Bazanov (see PK-62, 77) and Kacimov and Obnosov (2002) for empty ditches reconstructed by the specification of boundaries corresponding to *BMC* in the hodograph or other auxiliary planes (e.g., the plane of the Zhukovskii holomorphic function, which is defined as w–i z, see PK-62,77). We also recall the analytical and numerical solutions of Dagan (1964) and Gjerde and Tyvand (1992), who studied potential transient 2-D (not DF) flows towards horizontal drains (modeled by linear sinks and empty circles, correspondingly).

Curve 2 in Fig. 2b shows $A(Q_d)$. The cross-sectional area, A, of *BMC* (in Fig. 1a) is evaluated by the **NIntegrate** routine of *Mathematica* as:

$$A = -2\int_0^1 y(x)\,\mathrm{d}\,x\,, \tag{6}$$

Fig. 3 shows the results of modeling with HYDRUS-2D (Šimůnek et al., 2016). We selected $Q_d = 0.2/\pi$ in the analytical solution (3). With the help of eqs. (3) and (5) we generated 10 points on *MC*, imported them from *Mathematica* into HYDRUS, and made a spline curve in dimensional quantities used by HYDRUS. Also, HYDRUS uses *z* for the vertical coordinate. Fig. 3a shows the HYDRUS modeling domain bounded by an isobaric curve *MC*, for which we selected *L*=100 cm. Soil is loam from the HYDRUS soil catalog. The horizontal and vertical segments CA_h and MA_v in Fig. 3 are no-flow lines. We selected $L_A^* = 500$ cm, i.e., we assumed a quarter-circle A_hA_v with a radius of 500 cm to be a line with a constant piezometric head (we recall that HYDRUS, unlike PK-62,77 and Strack, 1989, uses *h* as a notation for the pressure head), along which we set $h_A^* = 32.2$ cm. This value was found at $r^* = 500$ cm for a selected value of Q_d^* from the logarithmic variation of $h^*(x^*)$ along *CA*, counting from the fiducial point *C* where $h_C^* = 0$, see eq. (2). Fig. 3b shows the isotachs (also constant h^* and ϕ^* contours), and Fig. 3c shows the streamlines. The origin of the spatial coordinates is retained in Fig. 3 to indicate the position of the generating sink. HYDRUS results match very well the analytical solution.

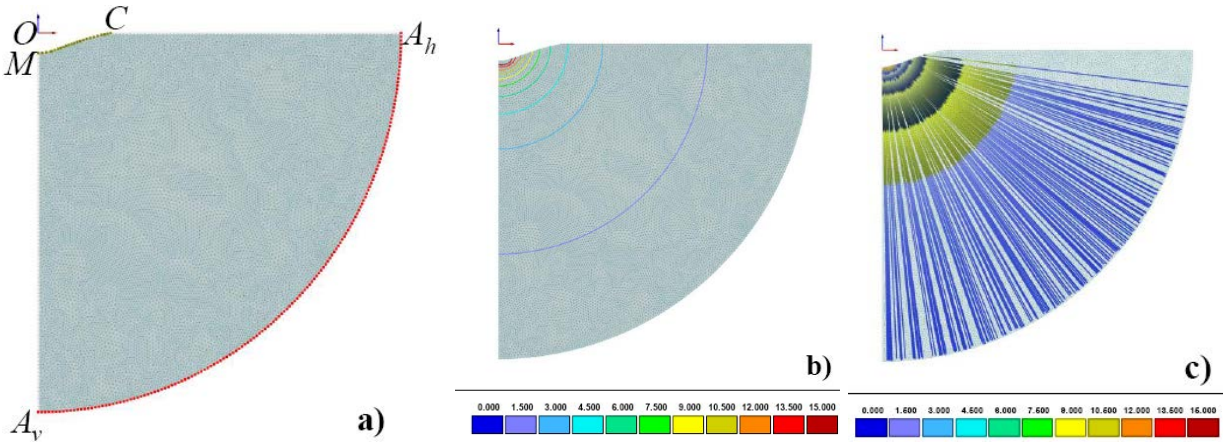

Fig. 3. The HYDRUS flow domain for a half-ditch generated by a line sink a), isotachs b), and streamlines c).

3. A Point-Sink-Generated Dimple Draining a Confined Aquifer

In this section, we use the same procedure as in Section 2 for the case of axisymmetric flow towards a depression *BMC* shown in Fig. 4 in an axial cross-section. We select a system of cylindrical coordinates $Oz^*\rho^*\kappa$, where z^* is a vertical coordinate (the same now as in HYDRUS-2D), $\rho^*=\sqrt{x^{*2}+y^{*2}}$, $r^*=\sqrt{\rho^{*2}+z^{*2}}$ and the angular coordinate κ vanishes from the analysis due to axial symmetry. At the origin *O*, we now place a point sink of intensity Q_d^* (m^3/s).

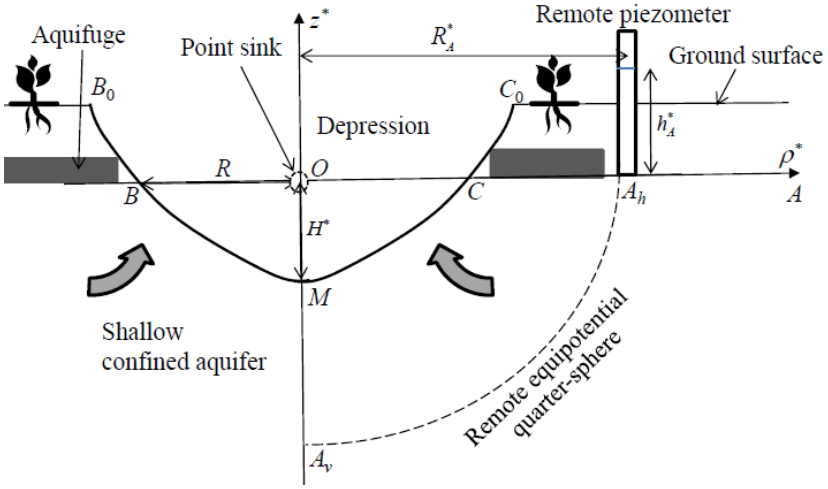

Fig. 4. An axial cross-section of an axisymmetric crater draining a confined aquifer.

The piezometric head caused by a point sink is (PK-62,77):

$$h^*=\frac{Q_d^*}{2\pi K_s}\left(\frac{1}{R}-\frac{1}{r^*}\right), \tag{7}$$

where *R* is the radius of the depression that coincides with the r^* (and ρ^*) coordinate of points *B* and *C* in Fig. 4. Eq. (7) sets up the total head equal to zero in these reference points. The depression of a depth H^* is empty and, therefore, the pressure head $p_{BMC}^*=0$ along this curve in Fig. 4 (a surface in 3-D). At a remote point A_h, located at a distance R_A^* ($R_A^* >> R$) from point *O* (Fig. 4), we have:

$$h_A^*=\frac{Q_d^*}{2\pi K_s R}. \tag{8}$$

Point A_h is a surrogate infinity of the infinite point A on the Riemann sphere. The head of eq. (8) is illustrated in a remote piezometer sketched in Fig. 4. We recall (PK-62,77) that for flow to a 3-D sink, the piezometric head at infinity is finite, unlike for a 2-D sink (Section 2), for which the head at infinity (point A) in Fig. 1b logarithmically blows up to infinity.

We introduce dimensionless quantities: $(H, z, \rho, r, h, p, h_A, R_A) = (H^*, z^*, \rho^*, r^*, h^*, p^*, h_A^*, R_A^*)$,

$Q_d = Q_d^* / (2\pi K_s R^2)$, $(V, u, v) = (V^*, u_\rho^*, v_Z^*) / K_s$, where (u,v) are now the radial and vertical velocity components.

From eq. (7), a zero-pressure isobar (seepage face) *BMC* is reconstructed, similarly to eq. (3), by an equation:

$$\rho = \sqrt{\frac{1}{(1 - z/Q_d)^2} - z^2}, \quad 0 \le \rho \le 1, \ -H \le z \le 0. \tag{9}$$

We note that some Martian hydrologists use the term “aquifer sapping face” and “crater wall” (Goldspiel and Squyres, 2011) for what is called a “seepage face” in terrestrial civil engineering (Strack, 1989).

Eq. (9) defines a quartic line. The depth H is found from eq. (9), which at $\rho = 0$ is reduced to a quadratic equation having the following physically meaningful solution:

$$H = \frac{\sqrt{Q_d^2 + 4Q_d} - Q_d}{2}. \tag{10}$$

We used eqs. (9-10) and calculated the volume of the depression *BMC* in Fig. 4 as a body of revolution:

$$V = \pi \int_{-H}^{0} \rho^2(z)\,dz = \frac{\pi Q_d}{6}\left(Q_d^{\,2} + 6Q_d + 6 - (4 + Q_d)\sqrt{Q_d(4 + Q_d)}\right), \tag{11}$$

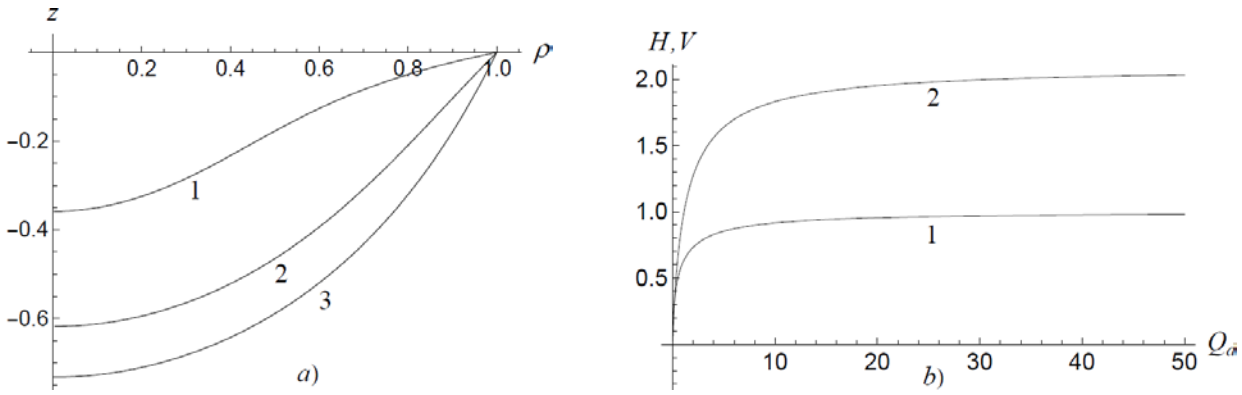

Fig. 5. a) Half-contours of a sink-generated axisymmetric topographic depression draining a confined aquifer for $Q_d = 0.2$, 1, and 2 (curves 1, 2, and 3, respectively). b) Depth and volume (curves 1 and 2, respectively) of an axisymmetric sink-generated depression in a confined aquifer.

Fig. 5a shows the isobars *MC* for $Q_d = 0.2$, 1, 2 (curves 1-3, correspondingly). In Fig. 5b, the curves (10) and (11) are plotted. Obviously, for $\lim_{Q_d \to 0} H = 1$ and $\lim_{Q_D \to \infty} V = 2\pi/3$, *BMC* becomes a hemisphere in this limit, while for small Q_d, we get a disk.

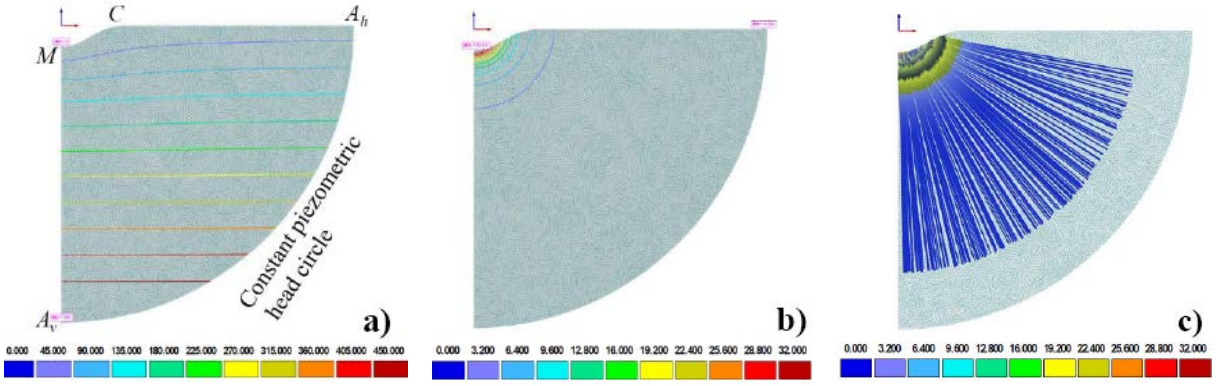

Fig. 6. HYDRUS isobars corresponding to $Q_d = 0.2$ a), isotachs b), and streamlines c).

The results of HYDRUS-2D simulations (in dimensional quantities) corresponding to the analytical case of $Q_d = 0.2$ are presented in Fig. 6. As in Section 2 (Fig. 3), we considered a loamy soil. We selected the radius *R* of the HYDRUS axisymmetric depression to be 100 cm. Using eqs.

339 (9) and (10), we generated ten discrete points on *MC* and made a HYDRUS spline (seepage face).
340 The radius R_A^* of a constant piezometric head quarter-circle A_hA_v was 500 cm. According to eq. (8)
341 the total head $h_A^* = p_{Ah}^* = 20$ cm at point A_h and, therefore, along A_hA_v, i.e., the HYDRUS pressure
342 head is p_{AV}^* =520 cm at point A_v. Fig. 6a presents steady-state pressure head isolines. Fig. 6b
343 illustrated isotachs and Fig. 6c plots the streamlines. Figs. 6bc perfectly fit the analytical solution.
344 In the next section, we focus on an opposite case of steady flow in a purely unsaturated
345 Gardner soil, albeit the same trick will be used, *viz.* we place a fictitious sink "in the air" and use
346 real isobars to construct topographic craters (dimples).
347
348 **4. An Isobaric Depression Reconstructed From Philip's Point-Sink Array and**
349 **HYDRUS-2D Simulations**
350 Analytical solutions of Sections 2 and 3 ignored flow in the unsaturated zone and the
351 capillary fringe, which are important in the case of small-scale drainage entities (Abit et al., 2008,
352 Silliman et al., 2002
353 In this section, we incorporate into an analytical quasilinear model all three physical
354 factors, which control seepage: the gravitational force on Earth or Mars, Darcian resistance of the
355 soil, and capillarity.
356 We use a constitutive relation for the phase conductivity:
357 $$k_{un} = K_s \exp[\alpha_p p^*], \quad (12)$$
358 where $k_{un}(p^*)$ for $p^* \le 0$ is an unsaturated hydraulic conductivity, α_p (const > 0) is the sorptive
359 number (1/m) (Gardner, 1958, see also Raats, 1973). J.R.Philip (1968) pioneered utilizing eqn. (12)
360 for modeling 2D and 3D unsaturated flows (see, e.g., Pullan, 1990, Raats et al., 2002). The soil
361 constant α_p is related to the VG-HYDRUS parameters α and n via well-known empiric relations
362 (Acharya et al., 2012); we used eqn. (10) from Ghezzehei et al. (2007).

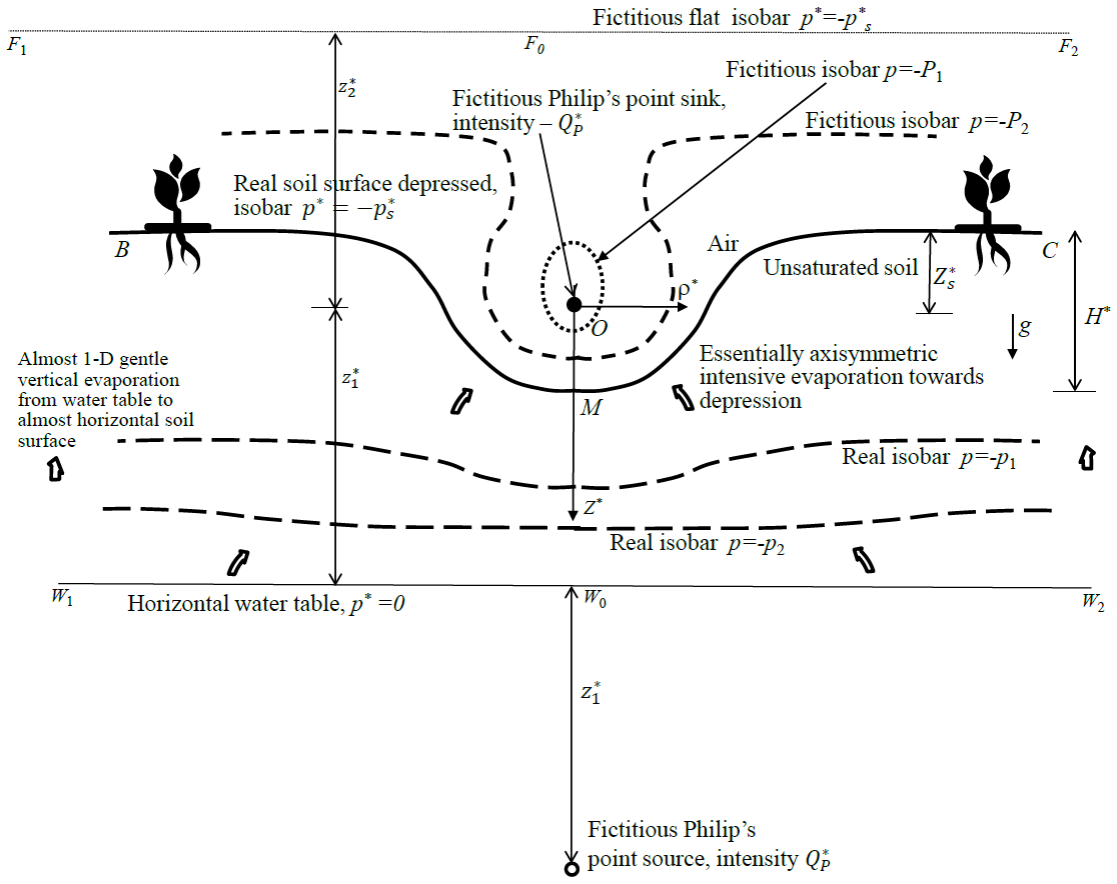

Fig. 7. An axial cross-section of evaporative flow in an unsaturated soil from a horizontal water table $W_1W_0W_2$ to a topographically depressed isobar *BMC*.

The evaporation arises from a steady upward flow from a horizontal (shallow) water table $W_1W_0W_2$ to a hot and dry soil surface *BMC* (Fig. 7) where the pressure head is constant ($p^* = -p_s^*$, $p_s^* > 0$). This surface has a topographic depression with the deepest point *M* at a depth $H^* > 0$ counted from the soil surface, which is horizontal and flat, far away from the topographic trough in Fig. 7, i.e., the water table is at a given depth b^* above a flat soil surface (near remote points *B* and *C*). *BMC* in Fig. 7 can also be related to the "sapping valleys" on Mars (see, e.g., Salese et al., 2019), albeit there is a difference in scales: the Martian depth of the water table $(Z_s^* - Z_1^*)$ is 4-5 km, while at SQU, the shallow groundwater table is only several tens of cm deep.

The depression in Fig. 7 is axisymmetric, like in Section 3. The axis of symmetry coincides

with the OZ^* axis of a cylindrical system of coordinates $OZ^*\rho^*$ (introduced similarly as in Section 3 above). To be consistent with Philip, we orient OZ^* downward.

Thus, unsaturated soil in 3-D is sandwiched between the $W_1W_0W_2$ plane and the soil surface obtained by the revolution of *BMC* with respect to the axis OZ^* in Fig. 7. There are no physical singularities representing drains, subsurface emitters, or plant roots in this soil layer.

The contour *BMC* in Fig. 7 is obtained in the following manner (Philip, 1989, Obnosov and Kacimov, 2018). A fictitious point sink of intensity Q_p^* (m^3/s) is placed at the origin of coordinates, such that the water table is beneath this sink at a depth of $Z_1^* > 0$. A fictitious horizontal isobaric plane $F_1F_0F_2$ is placed at the level $Z^* = -Z_2^*$, $Z_2^* > 0$, as illustrated in Fig. 7. At this plane, the pressure head $p^* = -p_0^*$ is specified. Points *B* and *C* in Fig. 7 of an "intermediate isobar" between two sandwiching isobaric planes $F_1F_0F_2$ and $W_1W_0W_2$ are at the level of Z_s^*, which can be either positive or negative. Fictitious point sources and sinks of intensity Q_p^* mirror each other with respect to the planes $F_1F_0F_2$ and $W_1W_0W_2$. Only the first fictitious source under the water table, placed on the OZ^* axis at a depth of $2Z_1^*$, is shown in Fig. 7. The array of an infinite number of such sinks-sources generates a family of isobars, some of which are real (two dashed lines $p^* = -p_2^*$, $p^* = -p_1^*$, $p_2^* < p_1^* < p_s^*$ are sketched in Fig. 7), and others are fictitious (two dotted lines $p^* = -P_2^*$, $p^* = -P_1^*$, $p_s^* < P_2^* < P_1^*$ are sketched in Fig. 7). Mathematically, instead of *BMC* in Fig. 7, we can select another soil surface, for example, any of the two dashed isobars.

Practically, we proceed in the following manner. One goes to the field with a theta-probe and collects the moisture content, θ_s, from the topsoil of a real depression, having a certain geometrical sizes b^*, H^*. If θ_s (and hence p_s^*) is almost constant in the depression and on a flat surface away from the depression, then the position (Z_1^*, Z_2^*) of the origin of coordinates (sink's

398 locus) and the strength Q_p^* of Zhukovskii's sinks-sources array should be mathematically adjusted
399 in such a manner that the physical (field) depression becomes close to a mathematical isobar *BMC*
400 in Fig. 7. In what follows, we illustrate this algorithm.

401 Routinely (see Philip, 1968, Raats, 1970, Obnosov and Kacimov, 2018), we introduce the
402 Kirchhoff potential, Ω^*, which is often called the matric flux potential:

403 $$\Omega^*(\rho^*, Z^*) = \int_{-\infty}^{p^*} k_{un}(u)\,\mathrm{d}u = k_{un}[p^*(\rho^*, Z^*)]/\alpha_P, \quad \Omega_\infty^* = K_s/\alpha_P, \tag{13}$$

404 i.e., Ω_∞^* is the Kirchhoff potential along $W_1W_0W_2$. Obviously, the lines of a constant Kirchhoff
405 potential are also isobars (the values of corresponding pressure heads are found directly from eq.
406 (13)) and isowetness curves (the corresponding water content is found from eq. (13) and the soil-
407 water retention function).

408 We introduce dimensionless quantities: $(z, b, H, z_s, z_1, z_2, \rho, r, h, p) =$

409 $(Z^*, b^*, H^*, \mathrm{Z}_s^*, \mathrm{Z}_1^*, \mathrm{Z}_2^*, \rho^*, r^*, h^*, p^*) \times \alpha/2$, $\Omega = \Omega^*/\Omega_\infty$, $Q_p = Q_p^*\alpha/\Omega_\infty$, $(V, u, v) = (V^*, u_p^*, v_Z^*)/K_s$

410 . Then Richards' equation (0) is reduced to a linear ADE:

411 $$\Delta\Omega^* = \alpha_P \frac{\partial\Omega^*}{\partial Z^*}, \quad u_\rho^* = -\frac{\partial\Omega^*}{\partial\rho^*}, \quad v_Z^* = \alpha_P\Omega^* - \frac{\partial\Omega^*}{\partial Z^*}, \tag{14}$$

412 where Δ is the Laplacian operator in (ρ,*Z*), u_ρ^* and v_Z^* are the radial and vertical velocity
413 components.

414 We adapt Philip's (1989) and Obnosov and Kacimov (2018) solutions to the case of flow in
415 Fig. 7 and obtain a series:

$$\Omega = \frac{\Omega_0\left[\exp[2(z_1+z_2)]-\exp[2(z+z_2)]\right]+\exp[2(z+z_2)]-1}{\exp[2(z_1+z_2)]-1} -$$

$$\frac{Q_P \exp z}{8\pi}\left[\frac{\exp(-r)}{r}-\frac{\exp(-r_1)}{r_1}-\frac{\exp(-r_2)}{r_2}+\frac{\exp(-r_3)}{r_3}+\frac{\exp(-r_4)}{r_4}\right]-\ldots, \quad (15)$$

$$r=\sqrt{\rho^2+z^2}, \quad r_1=\sqrt{\rho^2+(z-2z_1)^2}, \quad r_2=\sqrt{\rho^2+(z+2z_2)^2},$$

$$r_3=\sqrt{\rho^2+(z+2z_1+2z_2)^2}, \quad r_4=\sqrt{\rho^2+(z-2z_1-2z_2)^2},\ldots$$

where the constant $\Omega_0=\exp[-\alpha_p z_2],\ 0\le\Omega_0\le 1$ is the Kirchhoff potential along $F_1F_0F_2$. At points *B* and *C*, which are located on a physical isobar, whose remote «wings» are above the sink in Fig. 7, we have $\Omega=\Omega_s=\exp[-\alpha_p z_2]$ for $\Omega_0\le\Omega_s\le 1$.

The first term on the RHS of eq. (15) determines 1-D unsaturated evaporative flow from $W_1W_0W_2$ to $F_1F_0F_2$ in the layer $z_1<z<-z_2$. The terms in the square brackets of eq. (15) are responsible for sinks and sources, and consequently, for mirrored (imaged) with respect to the plains $z=z_1$ and $z=-z_2$. We emphasize that Philip (1989) and Obnosov and Kacimov (2018) studied flow for one real source representing a subsurface irrigation emitter, while all in Fig. 7 and eq. (15) are fictitious. A trick similar to ours was used by Zhukovskii (1948) in his famous formula for aerodynamics of ideal fluids. He combined mathematical singularities of a characteristic holomorphic function (two dipoles and vortex), the latter placed inside an airfoil (e.g., an impermeable cylinder). Zhukovskii also ignored a fictitious flow inside an airfoil (in the vicinity of the vortex) and only considered an exterior of a mathematical separatrix-streamline (cylinder). We confine real Darcian flow not by streamlines (for the sake of brevity, we have not even introduced the Stokes stream function, see Obnosov and Kacimov, 2018), but by two isobars (*BMC* and $W_1W_0W_2$ in Fig. 7).

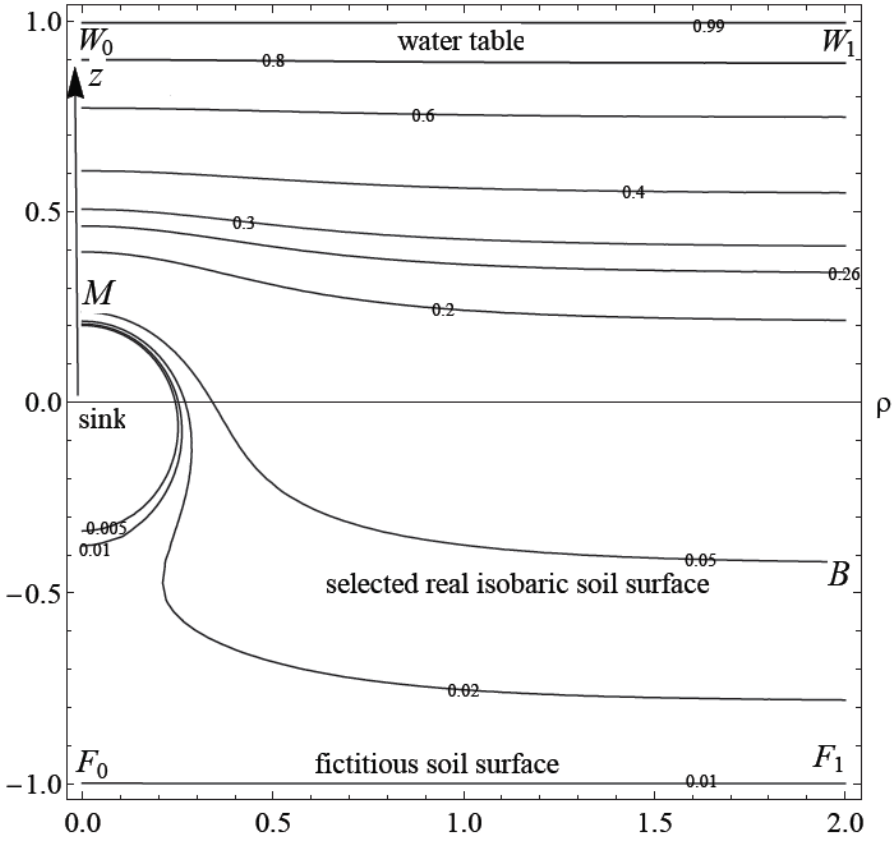

433

434 Fig. 8. Analytically computed isolines of Kirchhoff's potential for (z_1, z_2, Ω_0, Q_P) =(1, 1, 0.2, 1).

435

436 The results of computations based on eq. (15), where the series was truncated to 5 terms, are
437 plotted by the **ContourPlot** routine of *Mathematica* in Fig. 8 for (z_1, z_2, Ω_0, Q_P) =(1, 1, 0.2, 1). As
438 an example, in Fig. 8, we selected an isobar *BM* as the real depressed isobaric soil surface
439 maintained at the Kirchhoff potential $\Omega_s = 0.26$. For this isobar, we used the **FindRoot** routine of
440 *Mathematica* and evaluated $z_M = 0.389$, $z_B = z_s = -0.177$, i.e., the dimensionless depth of the
441 depression in Fig. 8 is H=0.566.

442 HYDRUS-2D simulations are presented in Fig. 9. We used silt loam with the VG-HYDRUS
443 triad of soil hydraulic parameters (α, n, K_s)=(2 1/m, 1.41, 1.08 m/day). We followed Ghezzehei et
444 al. (2007) and made Gardners's soil having $\alpha_P = 1.3\alpha n$, i.e., α_P=3.67 1/m. In Fig. 9a, a HYDRUS
445 axial section is shown for the case of the pressure head $p^*_{MC} = -0.82\,\mathrm{m}$. The flow domain, which

corresponds to the analytical depression, has the HYDRUS coordinates $z_M = -0.13\,\mathrm{m}$, $z_C = 0.23\,\mathrm{m}$, and $z_{W2} = -0.55\,\mathrm{m}$. The analytical isobar *MC* is converted to the HYDRUS spline curve similarly as in Sections 2 and 3. Figs. 9b and 9c show the HYDRUS isobars and streamlines. As is evident from Fig. 9c, the ditch funnels up the flux of moisture from the water table that also evaporates at the almost flat part of the soil surface (near point *C*). In other words, a simple flow tube is realized in Fig. 9c.

In Fig. 9d, we assumed a wetter soil surface having $p^*_{MC} = -0.63\,\mathrm{m}$. The origin of coordinates O is again, like in Figs. 8 and 9a, at the locus of the analytic imaginary sink. The geometry of the flow domain has changed as compared to Fig. 9a. The corresponding analytical depression MC has now the HYDRUS coordinates $z_M = -0.1\,\mathrm{m}$, $z_C = 0.176\,\mathrm{m}$, and $z_{W2} = -0.55\,\mathrm{m}$. The isobars are shown in Fig. 9d. They seem uninteresting, like ones in Fig. 9b. Fig. 9e presents HYDRUS streamlines, which are more interesting. Indeed, the flow topology is different from one in Fig. 9c. Specifically, like in Kacimov and Youngs (2005), who studied a seemingly trivial flow domain having a nontrivial two-sheet Riemann surface in the hodograph plane (see also Anderson, 2013). In Fig. 9e, we see a separatrix $S_sS_wS_d$, which divides the unsaturated domain into three subdomains. In the first one (counted from the left in Fig. 9e), moisture ascends from segment W_0S_w of the water table to the closest (deepest) section MS_d of the ditch surface (like in Fig. 9c). At the rest of the water table, segment S_wW_2, moisture descends (infiltrates) from S_sC on the soil surface (third subdomain). Point S_w is a stagnation point. Stagnation points and separatrix streamlines also appeared in Raats (1977) for steady flows to an array of the parallel line sinks in unsaturated Gardner soils. In HYDRUS, the numerical value of the velocity vector at this point (x=0.35 m) attains a sharp minimum (1.3×10^{-5} m/day).

The second, and most interesting, subdomain in Fig. 9e is bounded by the separatrix (streamline) and a curve segment $S_dH_pS_s$. Along this isobar (we recall that $p^*_{MC} = -0.63\,\mathrm{m}$, moisture

infiltrates into the soil through H_pS_s and exfiltrates back into the atmosphere through S_dH_p, making a U-turn. Therefore, the whole flow domain in Fig. 9e represents a complex flow tube similar to one in the potential flow shown in Fig. 62 of PK-77. It is noteworthy that in potential flows governed by the Laplace equation, this type of separatrix (complex flow tubes) emerges in situations when the boundary of the flow domain has three or more equipotential components. Figs. 9c and 9e illustrate that in ADE-governed unsaturated flow, a complex topology can appear in a domain bounded by two lines (surfaces) of a constant Kirchhoff potential.

A hinge point H_p in Fig. 9e is similar to ones in the classical Tothian (see, e.g., Kirkham, 1947, Toth, 2009) topology of purely saturated flows controlled by gravity, Darcian resistance, and topography of the isobaric ground surfaces (postulated by Toth), along which groundwater infiltrates-exfiltrates (but without taking into account unsaturated flow in the vadose zone). At the point H_p, the Darcian velocity vector is tangential to the soil slope. We rephrase: if the velocity vector is decoupled into the components normal and tangential to the local soil surface, then at H_p, the normal component is zero. Along S_dH_p, this normal component is oriented from the soil to the air, whereas along H_pS_s, the normal component points into the soil.

Summarizing, in the analysis of flow in an unsaturated soil represented in Fig. 9d and e, we amended the Tothian (2009) physical factors by capillarity of the soil. We then got a topological pattern shown (upside-down) at the forefront of the Freeze and Cherry (1979) and in a normal way in Figs. 2.25 – 2.26 of Radcliffe and Šimůnek (2010).

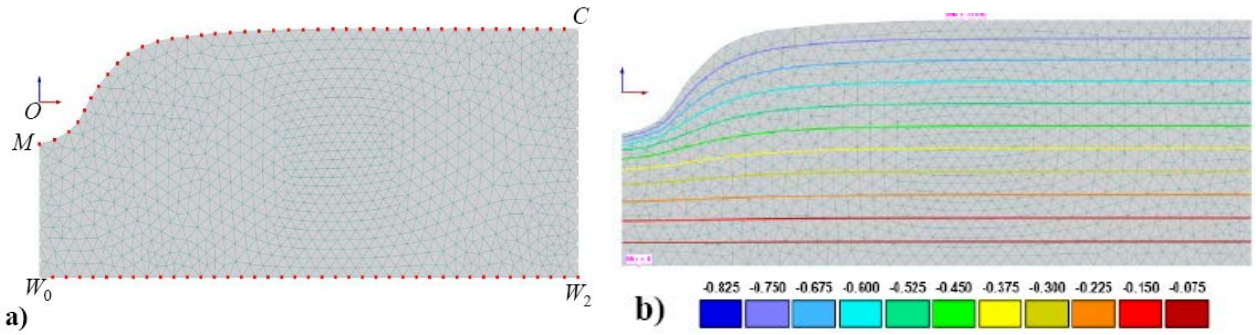

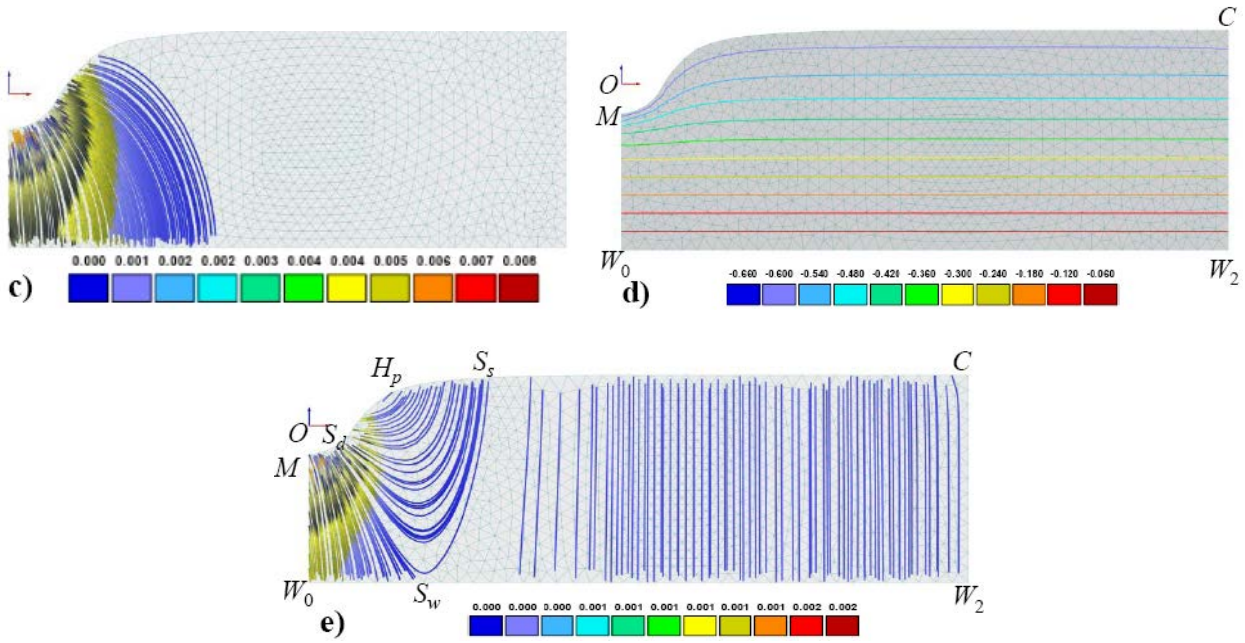

Fig. 9. HYDRUS simulations of purely unsaturated flow between a water table and an analytically found isobaric depression: a) finite element discretization of the flow domain and the boundary conditions, b) and d) pressure head contours, c) and e) streamlines. b) and c) flow to a relatively dry soil surface, d) and e) evaporation-infiltration at a relatively wet soil surface.

5. A Triangular Ditch in a Confined Aquifer

In this section, we return to steady, and capillarity-free flow in saturated soil. We consider 2-D potential flow in a vertical plane (Fig. 10a) and use the notations of Section 2, i.e., the complex physical coordinate is again $z^*=x^*+\mathrm{i}\,y^*$.

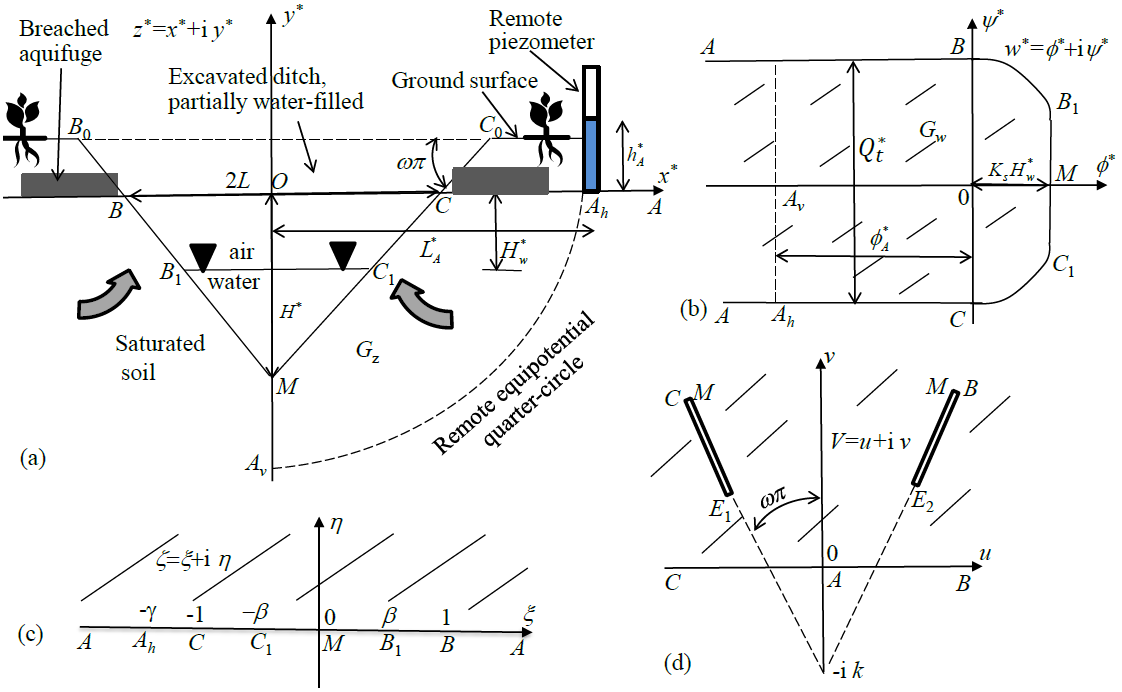

Fig. 10. A vertical cross-section of seepage flow towards a triangular ditch in a confined aquifer a), a complex potential domain b), a reference plane c), and a mirror-image in the hodograph plane d).

A caprock of a confined aquifer is now breached by a triangular isosceles ditch B_0MC_0, having a bank slope $\pi\omega$, $0 \le \omega \le 1/2$. The flow domain, G_z, is now the half-plane $y^* < 0$ with a triangular indent BMC. Ditch's depth is $H^* = L^* \tan \pi\omega$.

Unlike in Section 2, we allow water to accumulate in the ditch up the horizon B_1C_1 at the level H_w^*. The piezometric head at infinity (point A in Fig. 10ab) is infinite but, as in Section 2, we replace this infinity by a "surrogate infinity," *viz.* an equipotential line A_vA_h (shown as a dashed semi-circle and a segment in Figs. 10a and 10b, respectively). Practically, in a remote piezometer located distance L_A^* from the ditch axis, the total head, h_A^*, counted from points B and C, is measured. The overall flow rate into the ditch is Q_t^*. The domain G_w of the complex potential w is sketched in Fig. 10b. The boundary conditions for w are

$$\begin{cases} \phi^* = -K\, y^* \ \text{ along } \ BB_1 \text{ and } CC_1, \\ \phi^* = K\, H_w^* \ \text{ along } \ B_1M \text{ and } MC_1, \\ \psi^* = Q_t^*/2, \quad \text{along } \ AB, \\ \psi^* = -Q_t^*/2, \quad \text{along } \ AC. \end{cases} \tag{16}$$

To the dimensionless quantities introduced in Section 2, we add

$$(H_w, L_A, h_A) = (H_w^*, L_A^*, h_A^*)/L, \quad Q_t = Q_t^*/(K_s L).$$

We map the tetragon G_z onto a half-plane $\eta \ge 0$ of a reference plane $\zeta = \xi + \mathrm{i}\eta$ (Fig. 10c) with the correspondence of points $M \to 0$, $A \to \infty$, $B \to 1$, $C \to -1$, $B_1 \to \beta$, $C_1 \to -\beta$. Appendix I presents the details of our solution. An alternative method for the analytical solution (see the taxonomy of these methods in Aravin and Numerov, 1953, see also Bear, 1972) involves a conformal mapping of G_z onto a mirror-image of the pentagon in the hodograph plane. Fig. 10d sketches such a half-plane with two semi-infinite cuts for the case of an empty ditch.

Fig. 11 shows the function $Q_t(H)$ (curve 1) computed by eq. (A9) for $h_A = 3$ and $L_A = 5$. Similarly to Al-Shukaili et al. (2020b) and Kacimov (1985), we introduce the Morel-Seytoux dimensional seepage flow rate $\mu = Q_t^*/(K_s\sqrt{A^*})$, $A^* = H^* L^*$.

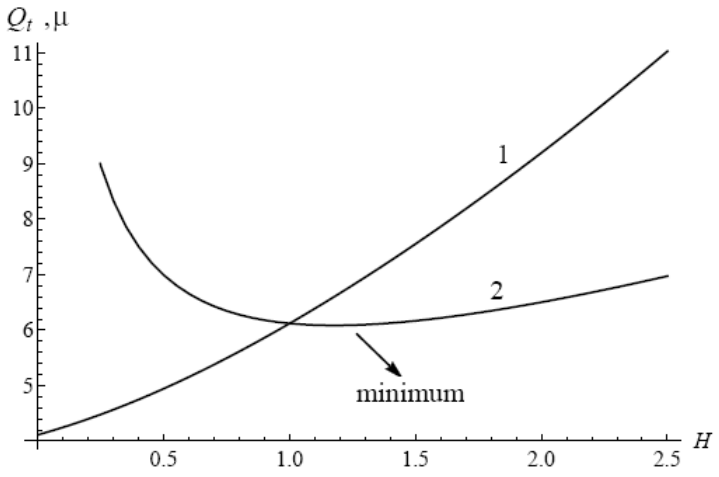

Fig. 11. Dimensionless seepage flow rates Q_t (curve 1) and μ (curve 2) as functions of H for an empty ditch, $h_A = 3$, and $L_A = 5$.

Curve 2 in Fig. 11 plots the function $\mu(H)$. The minimum of the function is $\mu \approx 6.085$ and $H \approx 1.177$. This minimum can be interpreted as a solution to the following optimal shape design problem, OSDP (similar to ones solved in Kacimov, 2005, 2006b):

OSDP 1. Determine an empty ditch, into which a minimal quantity Q_t^* of water seeps, provided the ditch area A^* and remote piezometric data (h_A^* and L_A^*) are fixed.

Curve 2 in Fig. 11 provides evidence that there is a unique and global solution to OSDP1. The minimum is "mild" (similar to ones in Kacimov, 1985), i.e., triangular ditches having slopes close to the best one will not deviate much from the best (minimal) seepage exfiltration rates. Problems similar to OSDP1 are common in civil engineering when a pit (e.g., for a building foundation) is excavated, and minimum exfiltration is desired, or pit's drainage measures are planned.

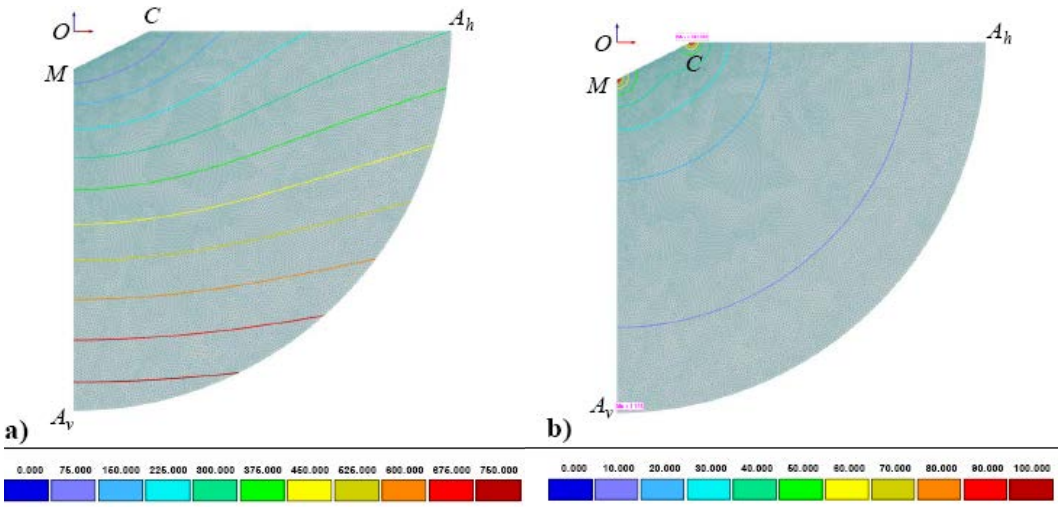

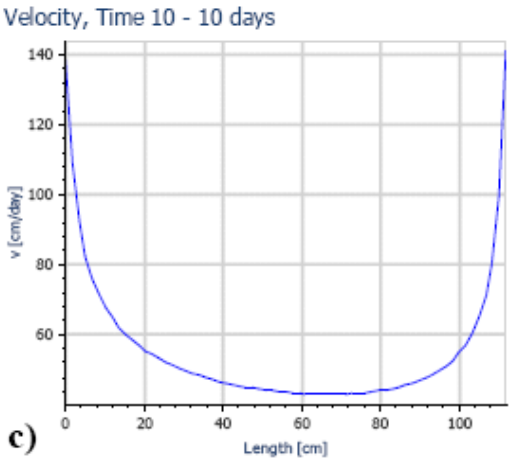

Fig. 12. HYDRUS simulations for a triangular empty ditch having H^*=50 cm, L^*=100 cm, L_A^* = 500 cm, and h_A^* =300 cm: isobars a), isotachs b), and Darcian velocities along the ditch side MC c).

For comparisons, in Fig. 12, we present the results of HYDRUS simulations for the tetrad of parameters (H^*, L^*, L_A^*, h_A^*) =(50 cm, 100 cm, 500 cm, 300 cm). Fig. 12a shows the isobars. Fig. 12b illustrates the isotachs. In the analytical solution, the Darcian velocity approaches infinity at points *M* and *C*. At the same time, it attains a minimal value, which corresponds to the tip of the cut in the hodograph domain (Fig. 10d). HYDRUS shows the same. In Fig. 12c, we plot the distribution of the velocities along the ditch side *MC*, where a minimum |*V*|=43.1 cm/day is attained at s_d =66.7 cm, where s_d is the arc coordinate counted from point *M* in Fig. 10a. Curves like the one in Fig. 12c are useful for the assessment of erosional stability of slopes of ditches, since heaving and suffusion are determined by exit values and directions of hydraulic gradient vectors $\vec{i}$. For example, PK-62,77 considers the condition $|\vec{i}|>1$ as a criterion of instability, according to which Fig. 12c illustrates that the ditch side *MC* in Fig. 12 is absolutely unstable at any s_d.

The HYDRUS-computed Morel-Seytoux factor μ is equal to 6.97 for the trench in Fig. 12, while the analytical solution gives μ =7.08. We computed other triangular ditches in HYDRUS-2D,

562 by using a discrete variation of the slope angle. We evaluated Q_t^* from the steady-state limit of the
563 cumulative flux into the ditch from a "feeding semicircle" (Fig. 10a, dashed curve). Then we
564 converted this dimensional Q_t^* into the dimensionless μ, which fits well the analytical curve 2 in
565 Fig. 11.

566 Collation of solutions for seepage into a triangular ditch and sink-generated ditch in Section
567 2 is done in the following manner. For the case presented in Fig.11, we use eq. (2) and evaluate
568 $Q_d = \pi h_A / \mathrm{Ln}\, L_A = 3\pi / \mathrm{Ln}\, 5 = 5.86$. The corresponding isobar is shown as curve 3 in Fig.2. Using
569 eq.(6) we evaluated the area and the Morel-Seytoux factor μ = 5.94. We surmise that this is a global
570 optimum in the class of arbitrary ditch shapes.
571
572

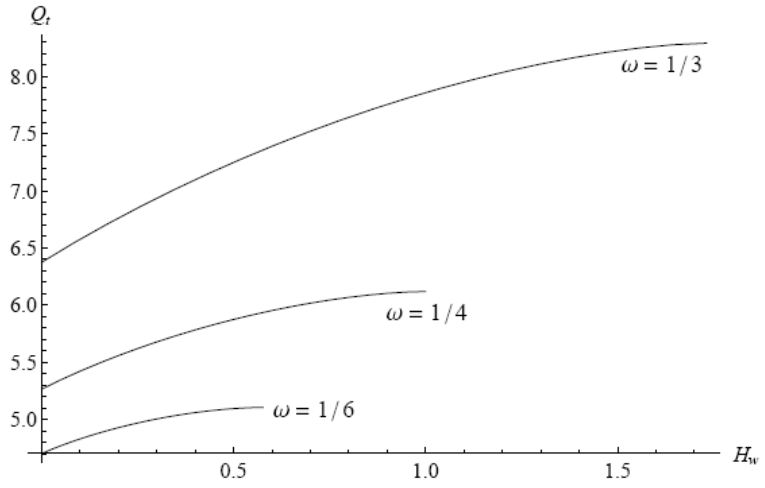

573

574 Fig. 13. The dimensionless seepage rate Q_t into a triangular partially filled ditch as a function of H_w
575 for three slopes (ω=1/6, 1/4, and 1/3), h_A=3, and L_A=5.
576
577 Next, we considered a general case of a partially-filled ditch (Fig. 10a). In Fig. 13, curves 1-
578 3 show the graphs of the functions $Q_t(H_w)$ for three ditch slopes: π/6, π/4, and π/3, and the same
579 $h_A = 3$ and $L_A = 5$ as in Fig. 11. In the regimes of partial filling, we can solve OSDPs similar to

OSDP1. Regional groundwater flow can be easily taken into account, similarly to Ilyinsky and Kacimov (1992b). The analytical solution to the steady problem can be readily extended to a transient regime of exfiltration into a gradually-filling ditch. We assume that the value h_A^* in Fig. 10a is high enough such that when we make a ditch, seepage into it does not reduce much h_A^*, and the soil in Fig. 10a remains saturated (an aquifer remains confined).

Let us assume, similarly as in HYDRUS, that during the transient seepage phase, the porous skeleton and water are incompressible. If evaporation from the ditch is ignored, then from the principle of mass conservation, the following ODE follows:

$$\frac{\mathrm{d}A_s^*}{\mathrm{d}t^*} = Q_t^*[H^*(t)], \tag{17}$$

where t^* is dimensional time and $A_s^*(t)$ is the area of the swelling triangle B_1C_1M in Fig. 10a (for comparisons see Al-Shukaili et al., 2020b, where emptying of triangular trenches has been studied). Obviously, the initial condition in eq. (17) is $A_s^*(0) = 0$, i.e., seepage-filling commences from an empty ditch stage. We put $A_s^*(t) = \left(H^* - H_w^*(\mathrm{t})\right)^2 \operatorname{cotan} \pi\omega$ into eq. (17) and get the following Cauchy problem:

$$2 \operatorname{cotan} \pi\omega \left(H_w^*(t) - H^*\right) \frac{\mathrm{d}H_w^*(t)}{\mathrm{d}t^*} = Q_t^*[H_w^*(t)], \quad H_w^*(0) = 0, \quad 0 < t < \infty. \tag{18}$$

We used the **NDSolve** routine of *Mathematica* to solve the nonlinear 1-st order ODE (18) numerically, with the RHS taken from eq. (A9). For this purpose, we interpolated 51 point values of $Q_t^*[H_w^*]$ (see curve 1) in the steady-state problem. The results of computations are shown in Fig. 13 in dimensionless quantities, to which we added a dimensionless time $t = t^* K_s / L$. In Fig.14, we plotted the functions $H_w(t)$ obtained from the solution of eq. (18) for $h_A = 3$ and $L_A = 5$, and the same ditch slopes ω = 1/6, 1/4, and 1/3, (curves 1-3, correspondingly). As is evident from these

601 draw-up curves, the ditches are filled out in finite time intervals, t_f =(0.115, 0.175, 0.24),
602 respectively. At $t > t_f$, seepage into a ditch continues due to an artesian pressure in an aquifer, and
603 exfiltrating water has to be removed (e.g., pumped out) if we want to keep points C and B in Fig.
604 10a at zero pressure heads (i.e., not ponded). That is equivalent to the condition that the horizon BC
605 remains static (see in Kacimov, 1991, a similar flow regime in a horizontal plane). The type of
606 curves in Fig. 14 can be used for the determination of K_s (similarly to Al-Shukaili et al., 2020b and
607 Kacimov, 2000b) that is also useful for deep structure constructors when pumping tests in deep
608 confined aquifers are not feasible. If an aquifer is unconfined, then for a suddenly emptied ditch (or
609 an auger hole, Kacimov 2000,b), $t_f = \infty$

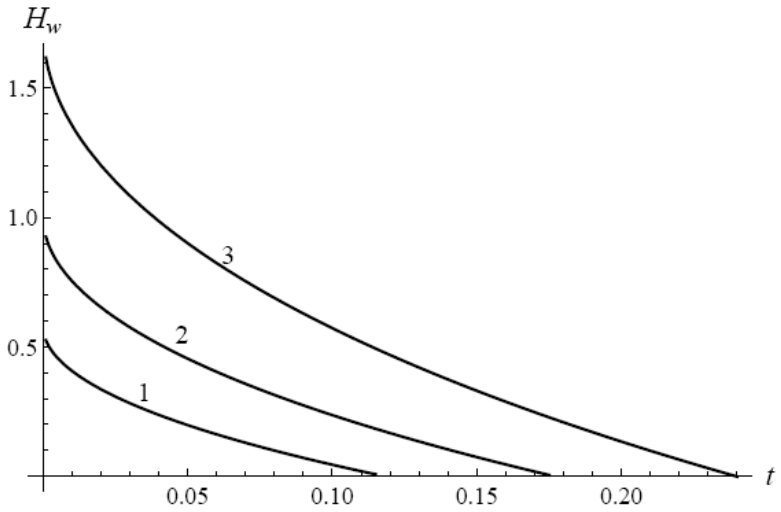

610

611 Fig. 14. Dimensionless draw-up curves H_w (1, 2, and 3) as functions of dimensionless time *t* for
612 different values of ω (1/6, 1/4, and 1.3,respectively).

613

614 A transient analytical solution can be compared with a numerical one, which involves a new
615 reservoir boundary condition of HYDRUS (Šimůnek et al., 2018). This new HYDRUS option
616 allows for the consideration of variable storage of a furrow channel, or well bore (e.g., Bristow et
617 al., 2020, Sasidharan et al. 2018, 2019, 2020), the contours of which are subject to the condition of
618 a constant piezometric head on the submerged part and a seepage face on the empty part of the

draining entity. HYDRUS then considers flow into or out of the reservoir through its interface with the subsurface transport domain depending on the prevailing conditions in the transport domain, such as the position of the groundwater table or piezometric heads, and external fluxes, such as pumping, or injection, or evaporation, or precipitation. The furrow reservoir can be adapted for our triangular ditch. The problem considered in Fig. 12 was rerun under transient conditions, starting with an empty ditch with dimensional sizes of H^* =50 cm and L^*=100 cm, corresponding to the case illustrated by curve 1 in Fig. 14. The HYDRUS draw-up curve $H_w^*(t^*)$ is shown in Fig. 15.

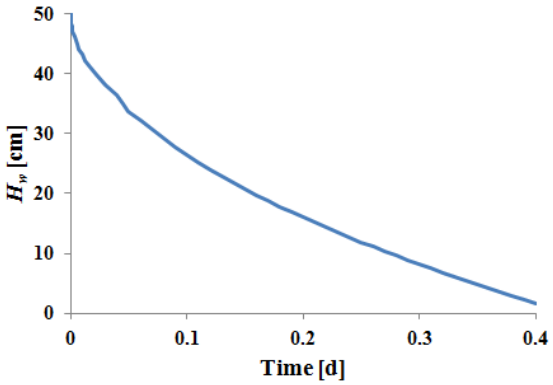

Fig. 15. A draw-up curve computed by HYDRUS for ω=1/6, H^*=50 cm, and L^*=100 cm.

There is a perfect match between the results in Fig. 15 and curve 1 in Fig. 14 from the analytical solution in dimensionless variables. We also compared the transient fluxes into the half-ditch, i.e., the analytical $Q_t/2$ from Fig. 11 (curve 1) and one computed by HYDRUS. For example, at t^*=0.1 day, the HYDRUS flux is about 6075 cm^2/day, whereas the analytical flux $Q_t^*/2$ is 6063 cm^2/day.

6. Comparison of Terrestrial and Martian Evaporating Spots

As an example, let us consider depression 1 (Q_d=0.2) in Fig. 5. Assume R^* =100 cm, H^*=35 cm, and a loamy soil having K_s=25 cm/day. Let the water evaporate from the disk πR^{*2} with a constant intensity e. In order to keep the crater empty, this value has to be $e = 0.2 \times 25/\pi \approx 1.6$

638 cm/day, which is - according to the Penman-Monteith equation and field measurements of
639 evaporation - a too high value even in the Empty Quarters of Oman.

640 If one wants to reconstruct desertification of Mars or intercept ascending moisture fluxes
641 from the deep water table, for example in projects of Mars colonization, then the topography like
642 the one in Fig. 9 should be taken into account similarly to what we have on Earth. Hummocky
643 terrains or even earth dams (Kacimov and Brown, 2015) generate complex 2D and 3D Toth-type
644 Darcian fluxes. Specifically, flat landforms with a homogeneous vadose zone and a shallow water
645 table are easy to examine for water storage and fluxes: it suffices to measure the depth of the water
646 table and the pressure head (moisture content) of the topsoil to infer what is the value and direction
647 of the flux. If the vadose zone is heterogeneous, the flux magnitudes can attain nontrivial extrema,
648 even of a simplest type of a two-layered soil (Kacimov et al., 2019). Fig. 9e illustrates that routine
649 measurements of the boundary condition on soil surfaces with depressions are not sufficient for the
650 determination of the directions and magnitudes of the motion of water governed by the Richards
651 equation.

652
653 **7. Concluding Remarks**

654 The mainstream groundwater hydrology focuses on MAR (Managed Aquifer Recharge), a
655 method of replenishing aquifers, especially in arid environments. We are putting forward the
656 opposite concept of MAD (Managed Aquifer Discharge) of shallow aquifers, which have to be
657 intelligently drained to mitigate the damage inflicted by groundwater inundation. The analysis in
658 this paper will be useful in planned drainage of water-logged built-up areas and further studies in
659 dryland ecohydrology (Camporeale et al., 2019). Maillart's desert ditches of Central Asia (similarly
660 as ones in humid Holland), can be viewed as a technique of lowering a shallow water table or
661 piezometric surface. The shape of these ditches can be mathematically approximated by isobars
662 made by hydrodynamic sinks, comparable with Zhukovskii's method of a smart composition of

663 singularities in aerodynamics. The Darcian flows governed by the Laplace equation in saturated
664 media or ADE for steady flows in unsaturated media can be viewed as created by intelligently
665 located singularities. The resulting isobars model the outlets in seepage to empty curvilinear ditches
666 and depressions. Seepage to triangular ditches, both empty and partially filled, is modeled by
667 conformal mappings and the BVP method. The transient stage of filling, i.e., the variable storage in
668 ditches, is examined by solving a Cauchy problem for a nonlinear ODE with type curves showing
669 how rapidly the ditch is filled up. HYDRUS-2D simulations well agree with analytical modeling.
670 Analytical solutions and HYDRUS reconstruct jointly isobars, isohumes, isotachs, and streamlines -
671 the theoretical arsenal of soil physicists and civil engineers working with Earth and Mars soil and
672 water systems. The proper design of ditches, pits, and other artificial excavations to be operated in
673 shallow water table environments, as well as understanding of subsurface hydrology of natural
674 wadis and depressions, can incorporate the findings of this paper.
675

676 **Appendix**

677 The Schwarz-Christoffel integral maps conformally the reference half-plane on G_z:

678 $$z(\zeta)+\mathrm{i}H=-\mathrm{c}_1(1-\mathrm{i}H)\int_0^{\zeta}(1-\tau^2)^{-\omega}\tau^{2\omega}\,\mathrm{d}\,\tau=-(1-\mathrm{i}H)\frac{\mathrm{B}_{\zeta^2}(1/2+\omega,1-\omega)}{\mathrm{B}(1/2+\omega,1-\omega)}, \qquad \text{(A1)}$$

679 where B and B_{ζ^2} are the complete and incomplete beta-functions, respectively (Abramowitz and
680 Stegun, 1969, formula 6.6.1). The positive constant $c_1=2/\mathrm{B}(1/2+\omega,1-\omega)$ in (A1) is determined
681 from the condition $z(1)=-1$. Note that $z(\zeta)$ obeys the symmetry condition $z(-\overline{\zeta})=-\overline{z(\zeta)}$ as it
682 should be.

683 From eq. (A1), along two seepage faces (BB_1 and CC_1), we have:

684 $$y(\xi)=H\left(\frac{\mathrm{B}_{\xi^2}(1/2+\omega,1-\omega)}{\mathrm{B}(1/2+\omega,1-\omega)}-1\right), \quad \beta\le|\xi|\le 1, \qquad \text{(A2)}$$

where $-\beta$ is the affix of point C_1. We determine β from the relation $y(-\beta) = -H_w$, that gives:

$$\frac{\mathrm{B}_{\beta^2}(1/2+\omega,1-\omega)}{\mathrm{B}(1/2+\omega,1-\omega)} = \frac{H-H_w}{H}. \tag{A3}$$

Next, we introduce a holomorphic function:

$$W(\zeta) = w(\zeta) - \frac{\mathrm{i}Q_t}{\pi}\arcsin\zeta. \tag{A4}$$

The function (A4), in accordance with (16) and properties of the function arcsin, satisfies the conditions:

$$\begin{cases} \mathrm{Re}\,W(\xi) = -y(\xi), & \xi \in (-1,-\beta)\cup(\beta,1), \\ \mathrm{Re}\,W(\xi) = H_w, & \xi \in (-\beta,\beta), \\ \mathrm{Im}\,W(\xi) = 0, & \xi \in (-\infty,-1)\cup(1,\infty). \end{cases}$$

Here $y(\xi)$ is determined in eq. (A2). Then the function $W_0(\zeta) = W(\zeta)/\sqrt{1-\zeta^2}$ obeys the following conditions along the ξ-axis:

$$\begin{cases} \mathrm{Re}\,W_0(\xi) = -y(\xi)/\sqrt{1-\xi^2}, & \xi \in (-1,-\beta)\cup(\beta,1), \\ \mathrm{Re}\,W_0(\xi) = H_w/\sqrt{1-\xi^2}, & \xi \in (-\beta,\beta), \\ \mathrm{Re}\,W_0(\xi) = 0, & \xi \in (-\infty,-1)\cup(1,\infty). \end{cases} \tag{A5}$$

Eqs. (A5) comprise a Riemann (Schwartz) BVP (Henrici, 1993, PK-62,77). The function $W(\zeta)$ is finite at two transition points $\xi = \pm 1$, continuous at points $\pm\beta$, and has a logarithmic singularity at infinity. Hence, the function $W_0(\zeta)$ has integrable singularities at points $\xi = \pm 1$ and vanishes at infinity. Therefore, the unique solution of the problem (A5) gives the Schwartz operator for the upper half-plane (Henrici, 1993, PK-62,77). Thus, after simple algebra, we get

$$W(\zeta) = \frac{2\zeta\sqrt{1-\zeta^2}}{\pi\mathrm{i}}\left(H_w\int_0^{\beta}\frac{\mathrm{d}\tau}{\sqrt{1-\tau^2}(\tau^2-\zeta^2)} - \int_{\beta}^{1}\frac{y(\tau)\,\mathrm{d}\tau}{\sqrt{1-\tau^2}(\tau^2-\zeta^2)}\right), \tag{A6}$$

where, for the sake of definiteness, the branch of the radical $\sqrt{1-\zeta^2}$ is fixed positive for $\zeta = \xi \in (-1,1)$ in the upper half-plane. This branch and, therefore, the function (A6) satisfy the symmetry condition $W(-\overline{\zeta}) = \overline{W(\zeta)}$. The integrals in (A6) are evaluated by the Sokhotski-Plemely formula: the first for $\zeta \to \xi \in (0,\beta)$, and the second for $\zeta \to \xi \in (\beta,1)$ (Henrici, 1993).

We illustrate the computations for the case of an empty ditch (H_w=H). We use the piezometric data at point A_h (Fig.10a), i.e., $\phi_A = -h_A$ First, from eq. (A1) along the ray CA we get:

$$x(\xi) = 1 + 2\sqrt{1+H^2}\int_1^{-\xi} (\tau^2-1)^{-\omega}\tau^{2\omega}\,\mathrm{d}\tau \,/\, \mathrm{B}(1/2+\omega, 1-\omega), \quad -\infty \le \xi < -1. \tag{A7}$$

From eq. (A5) we determine the affix $-\gamma$ of point A_h in the reference plane (Fig. 10c):

$$L_A = x(-\gamma). \tag{A8}$$

We use the **FindRoot** routine of *Mathematica* to solve eq. (A8) for γ. We put the found root of eq. (A8) into eq. (A6), and at $\phi_A = \phi(-\gamma) = -Q_t \log(\gamma + \sqrt{\gamma^2-1})/\pi + \mathrm{Re}\,W(-\gamma)$ arrive at the equality:

$$Q_t = \frac{2\gamma\sqrt{\gamma^2-1}}{\log(\gamma+\sqrt{\gamma^2-1})}\left(H_w \int_0^{\beta} \frac{\mathrm{d}\tau}{\sqrt{1-\tau^2}(\gamma^2-\tau^2)} - \int_{\beta}^{1} \frac{y(\tau)\,\mathrm{d}\tau}{\sqrt{1-\tau^2}(\gamma^2-\tau^2)} \right) - \frac{\pi\phi_A}{\log(\gamma+\sqrt{\gamma^2-1})}. \tag{A9}$$

Acknowledgments

This work was supported by Sultan Qaboos University via the grant “Rise of Water-table and Its Mitigation at SQU Campus” and it was carried out as part of the development program of the Scientific and Educational Mathematical Center of the Volga Federal District, agreement No. 075-02-2020-1478.. Helpful comments by two anonymous referees are highly appreciated.

721 **References**
722
723 +Abit, S. M., Amoozegar, A., Vepraskas, M. J., and Niewoehner, C. P. , 2008. Solute transport in
724 the capillary fringe and shallow groundwater: Field evaluation. Vadose Zone J., 7(3), 890-898.
725
726 +Abotalib, A. Z., and Heggy, E., 2019. A deep groundwater origin for recurring slope lineae on
727 Mars. Nature Geoscience, 12(4), 235.
728
729 +Abramowitz, M. and Stegun, I.A. 1969. Handbook of Mathematical Functions. Dover, New York.

730 +Abu-Rizaiza, O.S., 1999. Threats from groundwater table rise in urban areas in developing
731 countries. Water International, 24(1), 46-52.
732
733 +Abu-Rizaiza, O.S., Sarikaya, H.Z. and Khan, M.A., 1989. Urban groundwater rise control: case
734 study. J. of Irrigation and Drainage Engineering ASCE, 115(4), 588-607.
735
736 +Acharya, S., J. W. Jawitz, and R. S. Mylavarapu, 2012. Analytical expressions for drainable and
737 fillable porosity of phreatic aquifers under vertical fluxes from evapotranspiration and recharge,
738 Water Resources Research, 48, W125126, doi: 10.1029/2012WR012043.
739
740 + Afruzi, A., Nazemi, A. H., and Sadraddini, A. A., 2014. Steady-state subsurface drainage of
741 ponded fields by rectangular ditch drains. Irrigation and Drainage, 63(5), 668-681.
742
743 +Al-Rawas, A.A. and Qamaruddin, M., 1998. Construction problems of engineering structures
744 founded on expansive soils and rocks in northern Oman. Building and Environment, 33(2-3), 159-
745 171.
746
747 +Al-Sefry, S.A. and Şen, Z., 2006. Groundwater rise problem and risk evaluation in major cities of
748 arid lands–Jedddah case in Kingdom of Saudi Arabia. Water Resources Management, 20(1), 91-
749 108.
750
751 +Al-Senafy, M., 2011. Management of water table rise at Burgan oil field, Kuwait. Emir. Emirates
752 J. for Engineering Research, 16 (2), 27-38.
753
754 +Al-Senafy, M., Hadi, K., Fadlelmawla, A., Al-Fahad, K., Al-Khalid, A. and Bhandary, H., 2015.
755 Causes of groundwater rise at Al-Qurain residential area, Kuwait. Procedia Environmental
756 Sciences, 25, 4-10.
757
758 +Alsharhan, A. S., Rizk, Z. A., Nairn, A. E. M., Bakhit, D. W., and Alhajari, S. A. (Eds.), 2001.
759 Hydrogeology of an Arid Region: the Arabian Gulf and Adjoining Areas. Elsevier.
760
761 +Al-Shukaili, A., Al- Busaidi, H. and Kacimov, A.R., 2020a. Experiments, analytical and
762 HYDRUS2D modeling of steady jet of quasi-normal surface flow in rectangular channel coupled
763 with vertical seepage: Vedernikov-Riesenkampf's legacy revisited. Advances in Water Resources,
764 136, https://doi.org/10.1016/j.advwatres.2019.103503
765
766 +Al-Shukaili, A., Al- Mayahi, A., Al-Maktoumi, A. and Kacimov, A.R. , 2020b.
767 Unlined trench as a falling head permeameter: Analytic and HYDRUS2D modeling versus sandbox
768 experiment. J. Hydrology, 583, 124568.

+Al-Yaqout, A, and Townsend, F., 2004. Applicability of caliche (gatch) as liner/cover in arid climate landfills: Laboratory and field pad testing of permeability. Practice Periodical of Hazardous, Toxic, and Radioactive Waste Management. 8(4), 238-246.

+Attard, G., Winiarski, T., Rossier, Y. and Eisenlohr, L., 2016. Impact of underground structures on the flow of urban groundwater. Hydrogeology J., 24(1), 5-19.

+Anderson, E.I., 2013. Stable pumping rates for horizontal wells in bank filtration systems. Advances in Water Resources, 54, 57-66.

+Aravin, V. I., and Numerov, S. N., 1953. Theory of Fluid Flow in Undeformable Porous Media, Gostekhizdat, Moscow. Engl. Translation: 1965 by the Israel Program Scientific Translations, Jerusalem, Israel.

+Barron, O. V., Donn, M. J. and Barr, A. D. , 2013. Urbanisation and shallow groundwater: Predicting changes in catchment hydrological responses. Water Resources Management, 27, 95–115.

+Barua, G., and Alam, W., 2013. An analytical solution for predicting transient seepage into ditch drains from a ponded field. Advances in Water Resources, 52, 78-92.

+Bear, J., 1972. Dynamics of Fluids in Porous Media. Elsevier, New York. Elsevier, New York.

+Belotserkovsky, S. M., and Lifanov, I. K., 1992. Method of Discrete Vortices. CRC Press. (see also Белоцерковский, С.М., Лифанов, И.К., 1985. Численные методы в сингулярных интегральных уравнениях и их применение в аэродинамике, теории упругости, электродинамике. Москва, Наука).

+Bhardwaj, A., Sam, L., Martín-Torres, F. J., and Zorzano, M. P., 2019. Are slope streaks indicative of global-scale aqueous processes on contemporary Mars? Reviews of Geophysics, 57(1), 48-77.

+Boatwright, B. D., and Head, J. W., 2019. Simulating early Mars hydrology with the MARSSIM landform evolution model: New insights from an integrated system of precipitation, infiltration, and groundwater flow. Planetary and Space Science, 171, 17-33.

+Bob, M., Rahman, N., Elamin, A. and Taher, S., 2016. Rising groundwater levels problem in urban areas: a case study from the Central Area of Madinah City, Saudi Arabia. Arabian Journal for Science and Engineering, 41(4), 1461-1472.

+Bristow, K. L., J. Šimůnek, S. A. Helalia, and A. A. Siyal, Numerical simulations of the effects furrow surface conditions and fertilizer locations have on plant nitrogen and water use in furrow irrigated systems, Agricultural Water Management, 232, 106044, 11 p., doi: 10.1016/j.agwat.2020.106044, 2020.

+Camporeale, C., Perona, P., and Ridolfi, L., 2019. Hydrological and geomorphological significance of riparian vegetation in drylands. In "Dryland Ecohydrology" Ed. P.D'Odorico and A.Porporato, 239-275. Springer, Cham.

+Chahar, B. R., and Vadodaria, G. P., 2008. Drainage of ponded surface by an array of ditches. Journal of Irrigation and Drainage Engineering, ASCE, 134(6), 815-823.

+Chahar, B. R., and Vadodaria, G. P., 2012. Steady subsurface drainage of ponded surface by an array of parallel ditches. J. of Hydrologic Engineering, ASCE, 17(8), 895-908.

+Chaudhary, M.T.A., 2012. Implications of rising groundwater level on structural integrity of underground structures – investigations and retrofit of a large building complex. Structural Survey, 30(2), 111-129.

+Coda, S., Confuorto, P., De Vita, P., Di Martire, D. and Allocca, V., 2019. Uplift evidences related to the recession of groundwater abstraction in a pyroclastic-alluvial aquifer of Southern Italy. Geosciences, 9(5), 215, 1-15.

+Dagan, G. 1964. Linearized solution of unsteady deep flow toward an array of horizontal drains. J. of Geophysical Research, 69, 3361-3369.

+Duniway, M. C., Herrick, J. E., and Monger, H. C. , 2010. Spatial and temporal variability of plant-available water in calcium carbonate-cemented soils and consequences for arid ecosystem resilience. Oecologia, 163(1), 215-226.

+Edwards, C. S., and Piqueux, S., 2016. The water content of recurring slope lineae on Mars. Geophysical Research Letters, 43(17), 8912-8919.

+Freeze, R.A. and Cherry, J.A., 1979. Groundwater. Prentice-Hall Inc., Englewood Cliffs.

+Fujii, N. and Kacimov, A.R., 1998. Analytically computed rates of seepage flow into drains and cavities. International J. for Numerical and Analytical Methods in Geomechanics, 22, 277-301.

+Gardner, W.R., 1958. Some steady-state solutions of the unsaturated moisture flow equation with application to evaporation from a water table. Soil Science, 85, 228-232.

+Ghezzehei, T. A., T. J. Kneafsey, and G. W. Su, 2007. Correspondence of the Gardner and van Genuchten–Mualem relative permeability function parameters. Water Resources Research, 40, W10417, doi: 10.1029/2006WR005339, 2007.

+ Gjerde, K. M., and Tyvand, P. A. 1992. Transient free-surface groundwater flow due to an array of circular drainage ditches. Water Resources Research, 28(11), 2963-2972.

+Goldspiel, J. M., and Squyres, S. W., 2011. Groundwater discharge and gully formation on Martian slopes. Icarus, 211(1), 238-258.

+Goudie, A.S., 2013. Arid and Semi-arid Geomorphology. Cambridge University Press.

+Grimm, R. E., Harrison, K. P., and Stillman, D. E., 2014. Water budgets of Martian recurring slope lineae. Icarus, 233, 316-327.

+Grotzinger, J. P., Sumner, D. Y., Kah, L. C., Stack, K., Gupta, S., Edgar, L., ... and Milliken, R., 2014. A habitable fluvio-lacustrine environment at Yellowknife Bay, Gale Crater, Mars. Science, 343(6169).

+Gureghian, A. B., and Youngs, E. G. , 1975. The calculation of steady-state water-table heights in drained soils by means of the finite-element method. J. of Hydrology, 27(1-2), 15-32.

+Heilweil, V. M., and Watt, D. E., 2011. Trench infiltration for managed aquifer recharge to permeable bedrock. Hydrological Processes, 25(1), 141-151.

+ Henrici, P., 1993. Applied and Computational Complex Analysis. Volume 3: Discrete Fourier Analysis, Cauchy Integrals, Construction of Conformal Maps, Univalent Functions. Wiley, New York.

+Hobbs, S. W., Paull, D. J., and Clarke, J. D. A., 2014. A hydrological analysis of terrestrial and Martian gullies: Implications for liquid water on Mars. Geomorphology, 226, 261-277.

+Howard, K.W. and Israfilov, R.G. eds., 2012. Current Problems of Hydrogeology in Urban Areas, Urban Agglomerates and Industrial Centres (NATO Science Series, Vol. 8). Springer, Dordrecht.

+Hu, S., Lei, J., Xu, X., Song, Y., Tian, C., Chen, X., and Li, X., 2008. Theoretical analysis of the limiting rate of phreatic evaporation for aeolian sandy soil in Taklimakan Desert. Chinese Science Bulletin, 53(2), 119-124.

+Jha, A.K., Bloch, R. and Lamond, J., 2012. Cities and Flooding: a Guide to Integrated Urban Flood Risk Management for the 21st Century. The World Bank, Washington, DC.

+Ilyinsky, N.B. and Kacimov, A.R., 1992a. Problems of seepage to empty ditch and drain. Water Resources Research, 28(3), 871-877.

+ Ilyinsky, N.B., and Kacimov, A.R., 1992b. Analytical estimation of ground-water flow around cutoff walls and into interceptor trenches. Ground Water, 30, 901- 907.

+Kacimov, A.R. 1985. Optimization of the shape of a triangular unlined canal. Power Technology and Engineering. 19 (1), 41-43.

+Kacimov, A.R., 1991. Steady, two-dimensional flow of ground water to a trench. J. of Hydrology. 127, 71-83.

+Kacimov, A.R., 1992. Minimum dimension of total saturation bubble around an isolated source. Fluid Dynamics, 27, 886-889.

+Kacimov, A.R. 2000a. Circular isobaric cavity in descending unsaturated flow. J. Irrigation and Drainage Engrg. ASCE, 126(3), 172-178.

913 +Kacimov, A.R., 2000b Analytic solution for transient flow into a hemispherical auger hole. J.
914 Hydrology, v.228, 1-9.
915
916 +Kacimov, A.R.. 2005. Seepage to a drainage ditch and optimization of its shape. J. Irrigation and
917 Drainage Engrg. (ASCE), 132 (6), 619-622.
918
919 +Kacimov, A.R., 2006a. Analytic element solutions for seepage towards topographic depressions. J.
920 Hydrology, 318, 262-275.
921
922 +Kacimov, A.R., 2006b Analytical solution and shape optimisation for groundwater flow
923 through a leaky porous trough subjacent to an aquifer. Proceedings Royal Society London A,462,
924 1409-1423.
925
926 +Kacimov, A.R., 2007. Dipole-generated unsaturated flow in Gardner soils. Vadose Zone J., 6,
927 168-174.
928
929 +Kacimov, A.R., 2009. Minimal-seepage depth of isobaric cavity under ponded conditions.
930 J. Irrigation and Drainage Engrg. ASCE, 135 (1), 108-110.
931
932 +Kacimov, A.R., Al-Jabri, S., Sherif, M.M., Al-Shidi, S., 2009. Slumping of groundwater mounds:
933 revisiting the Polubarinova-Kochina theory and modeling by analytic element method.
934 Hydrological Sciences J., 54 (1), 174-188.
935
936 + Kacimov, A.R. and Brown, G., 2015. A transient phreatic surface mound, evidenced by a strip of
937 vegetation on an earth dam. Hydrological Sciences J. 60(2), 361-378
938
939 +Kacimov, A.R., and Obnosov, Yu.V., 2002. Analytical determination of seeping soil slopes of a
940 constant exit gradient. Zeitschrift fur angewandte Mathematik und Mechanik, 82(6), 363-376.
941
942 +Kacimov, A.R. and Obnosov, Yu.V., 2008. Leaky-layer seepage: the Verigin function revisited.
943 J. Engineering Mathematics, 62, 345-354,
944
945 +Kacimov A., and Obnosov, Yu.V., 2019. Modeling of 2-D Seepage from aquifer towards
946 stream via clogged bed: the Toth-Trefftz legacy conjugated. Advances in Water Resources. 129,
947 231–251.
948
949 + Kacimov, A., Obnosov, Yu.V. and Simunek, J. 2019. Minimizing evaporation by optimal
950 layering of topsoil: revisiting Ovsinsky's smart mulching-tillage technology via Gardner-Warrick's
951 unsaturated analytical model and HYDRUS. Water Resources Research, 55(5), 3606-3618.
952
953 +Kacimov, A.R., and Youngs, E.G., 2005. Steady-state water-table depressions caused by
954 evaporation in lands overlying a water-bearing substratum. J. Hydrologic Engrg. (ASCE), 10(4),
955 295-301.
956
957 +Kazemi, G.L., 2011. Impacts of urbanization on the groundwater resources in Shahrood,
958 Northeastern Iran: Comparison with other Iranian and Asian cities. Physics and Chemistry of the
959 Earth 36, 150–159.
960

+ Kereszturi, A., Möhlmann, D., Berczi, S., Ganti, T., Horvath, A., Kuti, A., Sik, A., and Szathmary, E. (2010). Indications of brine related local seepage phenomena on the northern hemisphere of Mars. Icarus, 207(1), 149-164.

+Kirkham, D., 1947. Studies of hillslope seepage in the Iowan drift area. Proceedings of the Soil Science Society of America, 12, 73-80.

+Kirkham, D., and Powers, W.K., 1972. Advanced Soil Physics. Wiley, New York.

+Kochel, R. C., and Piper, J. F., 1986. Morphology of large valleys on Hawaii—Evidence for groundwater sapping and comparisons with Martian valleys. J.of Geophysical Research, 91(B13), E175–E192.

+Kocurek, G., Westerman, R., Hern, C., Tatum, D., Rajapara, H. M., and Singhvi, A. K., 2020. Aeolian dune accommodation space for Holocene Wadi Channel Avulsion Strata, Wahiba Dune Field, Oman. Sedimentary Geology, 399, 105612.

+Kreibich, H., and Thieken, A.H. 2008. Assessment of damage caused by high groundwater inundation. Water Resources Research, 44, W09409.

+Lerner, D. N. ed., 2003. Urban Groundwater Pollution: IAH International Contributions to Hydrogeology 24. Balkema, Lisse.

+Lerner, D. N., and Harris, B, 2008. The relationship between land use and groundwater resources and quality. Land Use Policy, 26S (2009) S265–S273.

+Luo, W., Grudzinski, B., and Pederson, D., 2011. Estimating hydraulic conductivity for the Martian subsurface based on drainage patterns—A case study in the Mare Tyrrhenum Quadrangle. Geomorphology, 125(3), 414-420.

+Malin, M. C., and Carr, M. H., 1999. Groundwater formation of Martian valleys. Nature, 397(6720), 589-591.

+Malin, M. C., and Edgett, K. S. 2000. Evidence for recent groundwater seepage and surface runoff on Mars. Science, 288(5475), 2330-2335.

+Marra, W. A., Braat, L., Baar, A. W., and Kleinhans, M. G., 2014. Valley formation by groundwater seepage, pressurized groundwater outbursts and crater-lake overflow in flume experiments with implications for Mars. Icarus, 232, 97-117.

+Marra, W. A., McLelland, S. J., Parsons, D. R., Murphy, B. J., Hauber, E., and Kleinhans, M. G., 2015. Groundwater seepage landscapes from distant and local sources in experiments and on Mars. Earth Surface Dynamics, 3(3), 389-408.

+Medovar, Y.A., Yushmanov, I.O., and Bronskaya, E.E., 2018. Changes in the ecological condition of a territory at the construction of buildings with a deep foundation under various geological conditions in Moscow. Water Resources, 45(2), 65-72.

+Michalski, J. R., Cuadros, J., Niles, P. B., Parnell, J., Rogers, A. D., and Wright, S. P. , 2013. Groundwater activity on Mars and implications for a deep biosphere. Nature Geoscience, 6(2), 133-138.

+Mujica, C. R., and Bea, S. A., 2020. Estimations of rooting depths and sources of plant-available water (PAW) in flatland petrocalcic soils under different land uses. Geoderma, 361, 114019.

+Mukherjee, S., Singh, D., Singh, P., and Roy, N., 2020. Morphological and morphometric analysis of a topographic depression near Huygens basin, Mars: Identification of a putative endorheic playa. Geomorphology, 351, 106912.

+Naik, P.K., Tambe, J.A., Dehury, B.N. and Tiwari, A.N., 2008. Impact of urbanization on the groundwater regime in a fast growing city in central India. Environmental Monitoring and Assessment, 146(1-3), 339-373.

+Obnosov, Yu.V., and Kacimov, A.R., 2018. Steady Darcian flow in subsurface irrigation of topsoil impeded by substratum: Kornev-Riesenkampf-Philip legacies revisited. Irrigation and Drainage, 67(3), 374-391.

+Philip, J.R., 1968. Steady infiltration from buried point sources and spherical cavities. Water Resources Research, 4, 1039–1047.

+Philip, J.R., 1971. General theorem on steady infiltration from surface sources, with application to point and line sources. Soil Sci. Soc. Amer. Proc. 35, 867-871.

+Philip, J.R., 1989. Multidimensional steady infiltration to a water table. Water Resources Research, 25, 109-116.

+Polubarinova-Kochina, P.Ya., 1962. Theory of Ground Water Movement. Princeton University Press, Princeton. The second edition of the book (in Russian) was published in 1977, Nauka, Moscow.

+Porse, E., Glickfeld, M., Mertan, K., and Pincetl, S., 2016. Pumping for the masses: evolution of groundwater management in metropolitan Los Angeles. GeoJournal, 81(5), 793-809.

+Preene, M., and Fisher, S., 2015. Impacts from groundwater control in urban areas. Proceedings of the XVI ECSMGE, 2847-2852.

+Pullan, A.J., 1990. The quasilinear approximation for unsaturated porous media flow. Water Resources Research, 26(6), 1219-1234.

+Quan, R. S., Liu, M., Lu, M., Zhang, L. J., Wang, J. J., and Xu, S. Y., 2010. Waterlogging risk assessment based on land use/cover change: a case study in Pudong New Area, Shanghai. Environmental Earth Sciences, 61(6), 1113-1121.

+Raats, P.A.C., 1970. Steady infiltration from line sources and furrows. Soil Sci. Soc. Amer. Proc. 34, 709-714.

+Raats, P.A.C., 1971. Steady infiltration from point sources, cavities and basins. Soil Sci. Soc. Amer. Proc., 35, 689-694.

+Raats, P.A.C., 1972. Steady infiltration from sources at arbitrary depth. Soil Sci. Soc. Amer. Proc., 36, 399-401.

+Raats, P.A.C., 1977. Laterally confined, steady flows from sources and to sinks in unsaturated soils. Soil Sci. Soc. Amer. J., 41, 294-304.

+Raats, P.A., Smiles, D. and Warrick, A.W. eds., 2002. Environmental Mechanics: Water, Mass and Energy Transfer in the Biosphere. The Philip Volume. American Geophysical Union, Washington, DC.

+ Radcliffe, D.E., and Šimůnek, J., 2010. Soil Physics with HYDRUS: Modeling and Applications. CRC Press, Taylor & Francis.

+ Salese, F., Pondrelli, M., Neeseman, A., Schmidt, G., and Ori, G. G., 2019. Geological evidence of planet-wide groundwater system on Mars. J. of Geophysical Research: Planets, 124(2), 374-395.

+Sarmah, R., and Tiwari, S., 2018. A two-dimensional transient analytical solution for a ponded ditch drainage system under the influence of source/sink. J. of Hydrology, 558, 196-204.

+Sasidharan, S. A. Bradford, J. Šimůnek, B. DeJong, and S. R. Kraemer, 2018. Evaluating drywells for stormwater management and enhanced aquifer recharge. Advances in Water Resources, 116, 167-177, doi: 10.1016/j.advwatres.2018.04.003.

+Sasidharan, S., S. A. Bradford, J. Šimůnek, and S. R. Kraemer, 2019. Drywell infiltration and hydraulic properties in heterogeneous soil profiles. J. of Hydrology, 570, 598-561, doi: 10.1016/j.jhydrol.2018.12.073.

+Sasidharan, S., S. A. Bradford, J. Šimůnek, and S. R. Kraemer, 2020. Groundwater recharge from drywells under constant head conditions. J. of Hydrology, 583, 124569, 14 p., doi: 10.1016/j.jhydrol.2020.124569.

+Schirmer, M., Leschik, S., and Musolff, A., 2013. Current research in urban hydrogeology–A review. Advances in Water Resources, 51, 280-291.

+Silliman, S. E., Berkowitz, B., Šimůnek, J, and van Genuchten, M. Th. , 2002. Fluid flow and solute migration within the capillary fringe. Ground Water, 40(1), 76-84.

+Šimůnek, J., van Genuchten, M. Th. and Šejna, M., 2016, Recent developments and applications of the HYDRUS computer software packages, Vadose Zone J., 15(7), pp. 25, doi: 10.2136/vzj2016.04.0033.

+Šimůnek, J., Šejna, M. and van Genuchten, M. Th., 2018. New features of version 3 of the HYDRUS (2D/3D) computer software package. J. of Hydrology and Hydromechanics, 66(2), 133-142, doi: 10.1515/johh-2017-0050.

+Skaggs, R.W., Van Schilfgaarde, J., Bartels, J.M., Hatfield, J.L., Volenec, J.J. and Bigham, J.M. eds., 1999. Agricultural Drainage. American Society of Agronomy, Madison, WI.

+Skaggs, R. W., Youssef, M. A., and Chescheir, G. M., 2012. DRAINMOD: Model use, calibration, and validation. Transactions of the ASABE, 55(4), 1509-1522.

+Strack, O.D.L., 1989. Groundwater Mechanics. Prentice Hall, Englewood Cliffs.

+Strack, O.D.L., 2020. Applications of Vector Analysis and Complex Variables in Engineering. Springer, Cham.

+Tóth, J., 2009. Gravitational Systems of Groundwater Flow: Theory, Evaluation, Utilization. Cambridge University Press, New York.

+Vázquez-Suñé, E., Sánchez-Vila, X., and Carrera, J., 2005. Introductory review of specific factors influencing urban groundwater, an emerging branch of hydrogeology, with reference to Barcelona, Spain. Hydrogeology J., 13(3), 522-533.

+Vedernikov, V.V., 1939. Theory of Seepage and Its Application in Irrigation and Drainage. Gosstrojizdat, Moscow (in Russian)

+Vogwill, R. ed., 2016. Solving the Groundwater Challenges of the 21st Century (Vol. 22). CRC Press, Boca Raton.

+Wolfram, S. 1991. *Mathematica*. A System for Doing Mathematics by Computer. Addison-Wesley, Redwood City.

+Youngs, E. G., 1975. The effect of the depth of an impermeable barrier on water-table heights in drained homogeneous soils. J. of Hydrology, 24(3-4), 283-290.

+Youngs, E. G., 1990. An examination of computed steady-state water-table heights in unconfined aquifers: Dupuit-Forchheimer estimates and exact analytical results. J. of Hydrology, 119(1-4), 201-214.

+Youngs, E. G., 1994. Seepage to ditches from a ponded surface. J. of Hydrology, 161(1-4), 145-154.

+Zhukovskii, N. E., 1948. Collection of Works. Gostekhizdat, Moscow (in Russian).

Figure Captions

Fig. 1. A vertical cross-section of an empty ditch B_0MC_0 a); the right half of the empty ditch constructed such that the bottom of the ditch, *BMC*, is a seepage face of the flow in the domain G_z, generated by a fictive line sink at the origin O(x,y) b); the complex potential domain G_w for the whole ditch c).

Fig. 2. a) Half-contours of sink-generated ditches for Q_d = 0.2, 1, and 5.86 (curves 1, 2, and 3, respectively). b) The depth H of a sink-generated ditch and its area A (curves 1 and 2) as functions of seepage flow rate Q_d.

Fig. 3. The HYDRUS flow domain for a half-ditch generated by a line sink a), isotachs b), and streamlines c).

Fig. 4. An axial cross-section of an axisymmetric crater draining a confined aquifer.

Fig. 5. a) Half-contours of a sink-generated axisymmetric topographic depression draining a confined aquifer for Q_d = 0.2, 1, and 2 (curves 1, 2, and 3, respectively). b) Depth and volume(curves 1 and 2, respectively) of an axisymmetric sink-generated depression in a confined aquifer.

Fig. 6. HYDRUS isobars corresponding to Q_d = 0.2 a), isotachs b), and streamlines c).

Fig. 7. An axial cross-section of evaporative flow in an unsaturated soil from a horizontal water table $W_1W_0W_2$ to a topographically depressed isobar *BMC*.

Fig. 8. Analytically computed isolines of Kirchhoff's potential for (z_1, z_2, Ω_0, Q_P) =(1, 1, 0.2, 1).

Fig. 9. HYDRUS simulations of purely unsaturated flow between a water table and an analytically found isobaric depression: a) finite element discretization of the transport domain and the boundary conditions, b) and d) pressure head contours, c) and e) streamlines. b) and c) pure evaporation to a relatively dry soil surface, d) and e) evaporation-infiltration to-from a relatively wet soil surface.

Fig. 10. A vertical cross-section of seepage flow towards a triangular ditch in a confined aquifer a), a complex potential domain b), a reference plane c), and a mirror-image in the hodograph plane d).

Fig. 11. Dimensionless seepage flow rates Q_t (curve 1) and μ (curve 2) as functions of H for an empty ditch, h_A=3, and L_A=5.

Fig. 12. HYDRUS simulations for a triangular empty ditch having H^*=50 cm, L^*=100 cm, L_A^* = 500 cm, h_A^*=300 cm: isobars a), isotachs b), and Darcian velocities along the ditch side MC c).

Fig. 13. The dimensionless seepage rate Q_t into a triangular partially filled ditch as a function of H_w for three slopes (ω=1/6, 1/4, and 1/3), h_A=3, and L_A=5.

Fig. 14. Dimensionless draw-up curves H_w (1, 2, and 3) as functions of dimensionless time t for different values of ω (1/6, 1/4, and 1.3, respectively).

Fig.15. A draw-up curve computed by HYDRUS for ω=1/6, H^* =50 cm, and L^*=100 cm.

Abbreviations:

1) ADE = advective dispersion equation

2) BVP = boundary value problem

3) DF = Dupuit-Forchheimer

4) LHS, RHS=left hand side, right hand side

5) ODE = Ordinary Differential Equation

6) OSDP = Optimal Shape Design Problem

7) PK-62,77 = Polubarinova-Kochina, P.Ya., 1962. Theory of Ground Water Movement. Princeton University Press, Princeton. The second edition of the book (in Russian) was published in 1977, Nauka, Moscow.

8) VG = van Genuchten

HIGHLIGHTS

- Steady 2-D flows in a vertical plane and axisymmetric flows from a shallow horizontal water table to isobaric ditches (topographic depressions) are studied
- Method of images applied to the Laplace and advective dispersion equations, conformal mappings and HYDRUS-2D are utilized
- Saturated and unsaturated moisture motion in homogeneous soils is illustrated by isobars, isohumes, isotachs and streamlines
- Applications to arid zone hydrology on Earth and Mars are proposed